DOE/PC/89754--T2

DOE/PC/89754--T2

DE92 018755

PROJECT STATUS REPORT

Report Date: June 21,1989

Report No: 5

Report Period: 3/1/90-5/31/90

CONTRACT TITLE: The Kinetics of Sulfation of Calcium Oxide

CONTRACT NUMBER: DE-FG-22-89PC89754

CONTRACTOR NAME: M.I.T., 66-466
Cambridge, MA 02139

PRINCIPAL INVESTIGATORS: A.F. Sarofim and J.P.Longwell

CONTRACT PERIOD: February 27, 1989 to August 26, 1990

DISCLAIMER

1. INTRODUCTION.

Sulfur emissions from coal combustors must be controlled in order to comply with environmental standards. Many processes are available for this purpose, often involving the use of limestone as a sorbent.

Two principal types of coal-fired boilers exist in industry. One is the fluidized-bed coal combustor, that operates at relatively low temperature (ca.900°C), and has a long residence time (>2 hours). The other is a pulverized coal combustor, that operates at much higher temperatures (1200 to 1700°C), with a short residence time (<2 seconds) in the combustion chamber.

In both types, limestone compounds can be used for absorbing SO_2. In a first stage, limestone ($CaCO_3$) decomposes as it is heated to produce a porous CaO:

$$CaCO_3(s) \rightarrow CaO(s) + CO_2(g)$$

Sometimes, calcium oxide is also obtained from hydroxide or other salts. In any case, the reaction with SO2 occurs according to following overall reaction:

$$CaO(s) + SO_2(g) + 1/2\ O_2(g) \rightarrow CaSO_4(s)$$

This last reaction is the object of the present study.

The porous CaO is often represented as grains separated by pores (void volume), which can be filled as the grains grow on sulfation. The extent of this pore filling will depend on the grain size, the particle size, and porosity. For large particles, pore plugging occurs, which restricts the sulfate formation to the outer layer of the particle. The best conversion of $CaCO_3$ to $CaSO_4$ obtained in an industrial application is approximately 30% (Staudinger & Schröfelbauer, 1984).

Many different aspects of this gas-solid reaction have been discussed in the literature. The studies can be categorized into those investigating structural changes, chemical transformations and kinetic parameters

(1) Gas-solid structural models: Structural models have been developed to explain the retardation of the reactions by the $CaSO_4$ product layer. They usually assume a simple geometric description for the porous solid. The most common models are cylindrical pore or spherical grain models. They also assume simple Fickian diffusion through the product layer, which cannot model changes in diffusivities. A correct understanding of the models is important as they are used to calculate the kinetic parameters from conversion measurements. A good overview is given by Ramachandran & Doraiswamy (1982).

(2) The study of the chemical transformations occurring during the reaction: Calcium sulfate ($CaSO_4$) is the stable form of the product under the conditions used. This product, however, is not formed in one step. Low temperature studies (Ferguson & Rissmann, 1971; Van Houte et al, 1979) have demonstrated that calcium sulfite ($CaSO_3$) is formed as an intermediary product. It is then oxidized to the stable sulfate. At high temperature (>750°C), the product layer was found to be composed of calcium sulfate entirely, meaning that the oxidation rate is large enough to not be rate limiting (Marsh & Ulrichson, 1985.) The assumption of a single sulfate phase in the product layer is therefore justified.

(3) The kinetic parameters themselves and their value to predict reaction rates in real systems (Borgwardt, 1970, 1972, 1986; Hartman & Coughlin, 1974, 1976): Many studies have been conducted of the rate of limestone sulfation. However, the conditions (gas or stone composition) differ between studies, and the different structural models used to determine the parameters have

further complicated the comparison of kinetic parameters reported by various investigators. In addition, several authors point out that rate data are hard to reproduce (Hartman & Coughlin, 1976; Bhatia & Perlmutter, 1981a). As a result no unambiguous values for the kinetic parameters exist.

The rate of sulfation of a CaO surface is rapid at first, limited by the intrinsic kinetics, but slows down with increasing conversion as a consequence of the increased resistance to diffusion through the product layer. The sulfation rate of porous CaO, such as produced by the decomposition of limestone, is further reduced by diffusion within the pores and by the reduction of pore diameter. In small particles, this reduction occurs in a homogeneous manner throughout the solid until pore filling blocks further reaction. Large particles react faster at the pore mouths, where the product layer builds up faster, thus leading to pore mouth plugging. In both cases, the role of internal porosity is eliminated and the rate is controlled by diffusion through a layer covering the external surface of the particle.

The objectives of this study are to determine the intrinsic kinetics and the product layer diffusion rate by minimizing the resistances to gas-phase pore diffusion, and eliminating complications due to pore filling. This is achieved by the use of nonporous CaO. A wide range of particle sizes are used to change the relative importance of the regimes in which the intrinsic kinetics and product layer diffusion control. The assumption of constant product layer diffusivity can then be tested and the variables that determine this diffusivity independently studied. Information on product layer diffusion can also be obtained from studies of porous particles after the

pore mouths are all plugged and a uniform surface coating is obtained.

This information on diffusion rate and intrinsic reactivity can then be combined with a geometrical model to describe the rate of reaction over the entire range of conversions and is particularly useful in treating the effect of particle size on conversion history.

2. EXPERIMENTAL APPROACH

2.1. Choice of Samples

The four limes used in this study were (i) a combustion generated aerosol with an effective diameter of 0.02 μm, (ii) a synthetic lime with an average particle diameter of 0.3 μm, (iii) single CaO crystals with diameters of 15 to 20 μm, and (iv) calcined Iceland Spar with particle sizes of 10 to 15 μm. Table 1 summarizes their essential features.

The submicron CaO particles were produced by burning char particles containing atomically dispersed calcium. The calcium vaporized, oxidized in the vapor, and condensed to produce CaO aerosol with sizes <0.02μm (Graham, 1990). As shown in Figure 1, the grains are very spherical, hence easy to model. However, only low temperature measurements could be performed, due to the formation of calcium silicates (as the sample reacts with the quartz wool substrate) above 700°C. Nevertheless, the measurements provided useful information concerning initial rate and activation energy.

The next size range was generated using the citric acid technique, developed by Marcilly et al. (1972). A synthetic lime composed of very porous

particles (porosity between 90 and 95%), featuring non-porous, spherical granules with average diameter of 0.3 μm (see Figure 2), which translates into a surface area of about 5 m^2/g, is formed. The pore size distribution of this synthetic lime is shown in Figure 3. The porosity is restricted to the macropores between primary particles. Although the aggregates can be as large as 100 μm in diameter the porosity is so large that the effectiveness factor is close to one (0.97), so that the primary particles of 0.3 μm in diameter can be used to interpret the kinetic data. The physical structure can be varied within a limited range by modifying the preparation conditions. Table 2 gives an overview of the major structural parameters, and Figure 3 shows the pore size distribution of these samples.

Calcium oxide single crystals were used to investigate the rate of large, nonporous materials. This sample, obtained from Goodfellow Metals, Cambridge, England, is kept in an organic liquid in order to avoid hydration. Before use, it is ground and sieved to particle sizes of 15 to 20 μm (Mess, 1989). The advantage of this sample is that its structure is readily recognizable on SEM pictures (Figure 2), and therefore the formation of a product layer can be followed easily. Hydration, however, is unavoidable, but because of the large size of the grains used, it contaminates only a thin surface layer. Hence, the hydroxide layer will influence the results only at low conversions.

The fourth sample was produced from Iceland Spar, a crystalline $CaCO_3$ found in nature in a very pure form. Particles ranging between 10 and 15 μm in size were calcined by ramping the temperature to 800°C at a rate of

40°C/min in Helium to yield a porous CaO, with a porosity of 46%, and a surface area of 30 m^2/g (see SEM picture, Figure 2 and pore size distribution in Figure 4.) Product layer diffusion information was obtained from the conversion rate after the pores had been filled.

2.2. Experimental Procedure

The major piece of equipment used is a thermogravimetric analyzer. The thermal balance, manufactured by Cahn Instruments, is sketched in Figure 5. It is described in detail by Floess (1985). The balance itself is held under a constant He flow, to avoid contact of the corrosive SO_2 gas with the delicate electronics. The optimal flow rate through the balance was found to be 200 standard cubic centimeters per minute. A higher rate would create large temperature gradients around the sample pan. A lower rate would yield mass transfer limitations from the gas bulk to the pan surface (see also Floess). The gas used typically consists of 5% O_2, 3000 ppm SO_2 and a balance of helium. Helium was chosen rather than nitrogen because of the higher diffusivity it provides for SO_2 and O_2. The sample size had to be chosen smaller than 1 mg in order to avoid SO_2 depletion in the gas stream.

It was found that in some cases the product layer structure was a function of the experimental conditions. For purposes of determining the reaction order, samples were sulfated to a given conversion under standard conditions (typically 3000ppm SO_2, 5%O_2 at 800°C). The gas phase concentration could then be changed to examine the effect of concentration on the rate for a given product layer structure. An example of such a series of runs, designated as combination runs, at 800°C, and with 5% O_2, is shown in Figure 6.

As the sample sizes employed in the TGA were too small for purposes of sample characterization, larger amounts of CaO were sulfated in a separate, differential 1 cm diameter packed bed. The gas concentrations and temperatures used duplicated those in the TGA experiments. Surface areas were subsequently measured with nitrogen adsorption, and porosity with mercury intrusion.

Electromicrographic pictures were also made on a regular basis to provide qualitative information on the product layer structure. Approximate quantitative information of crystal sizes were obtained.

3.RESULTS AND DISCUSSION

3.1. Effect of Sample Type

The rates observed in the TGA using different types of samples vary widely depending on their physical structure. An overview of this is given in Figure 7. The early part of the conversion is controlled by surface reaction, and is proportional to the surface area. When the product layer thickness grows, diffusion through this layer becomes rate limiting. For small particles, this transition occurs at large conversion (needed to obtain the same thickness), while for the largest, almost no surface reaction rate can be measured.

The single crystal samples exhibit the slowest rate. Their surface area is very small since they consist of large (15-20μm), nonporous grains. Iceland Spar, which most resembles natural lime, exhibits a fast rate up to almost 40% conversion, at which point it suddenly drops. This corresponds most likely to the pore filling phenomenon described earlier. The sulfation of the submicron CaO particles, because of their high specific surface area, yield an extremely fast rate. The conversion behavior shown in Figure 7 was

obtained at 600°C because no accurate measurements could be performed at higher temperature (the response time of the TGA, especially when small sample weights are used is 30 seconds at best). The synthetic lime sulfation exhibits a much smoother behavior, than the three other samples. It provides useful information for both initial rate and product layer diffusion. Conversion measurements obtained at different temperatures with the synthetic lime are shown in Figure 8; Single crystal results in Figure 9.

Inasmuch as the surface area is an important parameter to predict the sulfation behavior, we first discuss how the surface area was observed to change as a result of sulfation.

3.2. Surface Evolution During Sulfation

Although extensive work has been done on the reduction of surface area of the lime during calcination (Glasson, 1958; Fischer, 1953; Bardakci, 1979; Hartman & Trnka, 1980; Hartman & Pata, 1978), the surface area behavior during sulfation is usually assumed to follow the prediction of any of the structural models (grain or pore models.)

Surface area data were obtained with the synthetic lime after sulfation for various periods of time at 800°C. The results are shown in Figure 10. In the absence of sintering, a surface area reduction is expected. It can be calculated rather easily using the simple grain model (justified by the granular structure featured by this sample). Following relationship between external specific surface area, S_X' and conversion, X, is found

$$S_X' = \frac{3}{[X(Z-1)+1]^{1/3}\, r_o\, [\rho_R(1-X) + \rho_P X]} \qquad (1)$$

where r_o is the initial grain radius and Z is the molar volume ratio of

product and reagent (Z=2.72). The densities are ρ_R for CaO (3.32 g/cm^3), and ρ_P for $CaSO_4$ (2.96 g/cm^3). The result is plotted on Figure 10, using the rate behavior observed in the TGA to relate time and conversion. The observed surface area is systematically lower than predicted, leading to the conclusion that sintering is occurring.

In order to model the observed behavior, the empirical approach suggested by Ranade & Harrison (1979) is used:

$$S_X' = S_{X\infty}' + (1-X)^m * (S_o' - S_{X\infty}') \qquad (2)$$

where $S_{X\infty}'$ is the final, lowest surface area measured, and S_o' is the initial surface area. The result is also presented in Figure 10. The best value for m was found to be m=3 in all cases, in accordance with the observations of Ranade & Harrison.

3.3. The Surface Kinetic Rate

The initial rate, taken per unit CaO mass, at 800°C, and with 3000ppm SO_2 and 5% O_2, is presented in Figure 11 as a function of the sample surface area, for various samples. From this type of plot, one can determine an average value for the rate per unit surface area ($8.4*10^{-6}$ mol/s m^2 under these conditions.)

An Arrhenius plot (Figure 12) can be drawn from measurements at different temperatures, performed under 3000ppm SO_2 and 5% O_2. Several series experiments are presented here. Three series were performed with synthetic lime (R1088, R1189, and R489), and one series with submicron ash. The activation energies are reasonably similar with an average value of 18 kcal/mol.

The rate can be expressed as

$$F = 2.5*10^{-2} \exp(-18\ (\text{kcal/mol})\ /RT)\ (\text{mol/s-m}^2) \quad (3)$$

Figure 12 shows that, even though a bit low, these results compare well with other authors.

The dependence of the rate on the SO_2 concentration is shown in Figure 13. The data can be fitted with an order of 0.52 on the SO_2 partial pressure, in good agreement with the value of 0.57 published by Borgwardt et al (1986) and by Gopalakrishnan et al. (1990).

In the absence of any product layer, the mechanism of sulfation involves chemisorption on the CaO surface (Low et al., 1971; Siriwardane, 1987). While the large range of partial pressures where the low order is observed precludes the use of a Langmuir-Hinshelwood isotherm, other adsorption isotherms (Freundlich), where the heat of adsorption is a function of surface coverage, could explain this phenomenon (Szekely et al., 1976).

3.4. Product Layer Diffusion

As soon as the product layer becomes sufficiently thick, diffusional processes become controlling. Comparison of the rates per unit surface area as a function of conversion for the different samples is shown in Figure 14. The rates vary widely because the product layer thickness, at a given conversion, is largest for the larger particles. These data are used to infer product layer diffusivities. Because of the definition of diffusion coefficient as the ratio of diffusion rate and concentration gradient, one must first decide what the diffusing species are.

3.4.1. Theoretical Description of Solid State Diffusion

The product layer diffusion, is usually described using the gas concen-

tration gradient as driving force, as if gaseous diffusion was occurring through a microporous layer. Borgwardt et al. (1986), however, used the observed high activation energy for diffusion to argue that the sulfur must be diffusing in an ionic form through the solid, nonporous product layer.

Ionic Diffusion

Ionic diffusion is a complex phenomenon that has been studied extensively (Jost, 1952; Fröger, 1964; Kingery et al, 1976; Shewmon, 1983), in the context of metal oxidation. No mechanistic studies of diffusion through $CaSO_4$ were found. The closest information available is the study of C and O diffusion through $CaCO_3$ crystals (Kronenberg et al., 1984). The mechanism for solid state diffusion can be viewed as the countercurrent diffusion of ions and defects. The diffusion of ions will either create a potential field (Cabrera & Mott, 1949), or induce the diffusion of other ions (or defects) in order to maintain a charge balance. As the diffusion rates are coupled, the slowest diffusing species is rate-controlling.

An additional complication arises from the fact that several independent diffusion paths can exist simultaneously. As the diffusion is dependent on the concentration of defects, some regions, where larger amounts of defects are present (dislocations, crystal boundaries), provide a faster diffusion path than the bulk. As a result, the diffusion step must be described as a parallel connection of different resistances. The path that provides fastest diffusion controls the rate.

Concentration Gradient

In order to obtain a value for the solid state diffusivity, using Fick's

first law for diffusion, the gradient in concentration of the rate-limiting species must be known. Since this information is not available, a general approach is suggested. At first, only one diffusion path is considered. A dimensionless concentration, γ, is defined as the molar ratio of the rate-limiting diffusing species to the calcium concentration in the product layer. In order to visualize its meaning, one can assume that SO_4^{--} is the rate-limiting diffusing species (Figure 15). In this case, the value of γ is the ratio $[SO_4^{--}]/[Ca^{++}]$, or S/Ca. A S/Ca, or γ gradient must be present.

The value of the parameter γ at both ends of the product layer is limited by thermodynamic equilibrium. The true value can be different from the equilibrium condition if the surface chemical reaction is slow compared to the product layer diffusion rate. In what follows, this reaction rate is assumed fast such that only the product layer diffusion is controlling.

At the outer surface, $CaSO_4$ is in equilibrium with the gas phase, that contains SO_2. We call this equilibrium γ_s^*. In the example of sulfate ions diffusing, γ is limited by the stoichiometric composition, or unity. At the opposite side of the product layer, the same reasoning applies. The limiting value, defined as γ_i^*, is determined by the constraint of thermodynamic equilibrium of $CaSO_4$ and CaO. In the example, γ_i^* is close to one as well, yet smaller than one.

As the calcium concentration in the product layer is a constant (equal to the molar density, ρ_{CaSO4}), the gradient in concentration of the rate-limiting species is equal to the gradient in the dimensionless value γ times the value of ρ_{CaSO4}. The diffusion step can thus be described with Fick's first law as proportional to the gradient of γ.

Calculation of the Diffusivity

As the overall reaction rate is the sum of the rates in each diffusion path, the rate of diffusion through the product layer is expressed as follows, with X as the conversion, and t the time

$$dX/dt = \Sigma \, (D_{sj} \, d\gamma/dr \, S_j(r)) \, \rho_P/\rho_R \qquad (4)$$

Where ρ_P and ρ_R are the molar density of Ca in the product layer and in the solid reagent, respectively (in mol/m^3). The surface area for path j at radial position r (coordinate perpendicular to the surface) per unit volume in the particle is expressed by $S_j(r)$ (m^{-1}) and D_{sj} (m^2/s) is the solid state diffusivity describing the diffusion in path j, using the gradient of γ as driving force. In reality, the rate-limiting diffusing compound can vary for different paths, and hence the gradient $d\gamma_j/dr$. However, since the true gradients are unknown, the use of a single value is a reasonable approximation, that simplifies the mathematical expression. An average value for the diffusivity can be defined as

$$D_s = \Sigma \, (D_{sj} \, S_j/S) \qquad (5)$$

assuming that S_j/S is independent of r.

The rate expression in the diffusion-limited regime becomes thus

$$dX/dt = D_s \, d\gamma/dr \, S(r) \, \rho_P/\rho_R \qquad (6)$$

with boundary conditions

$$\gamma = \gamma_s^* \qquad \text{at } r = r_s \qquad (7)$$

$$\gamma = \gamma_i^* \qquad \text{at } r = r_i \qquad (8)$$

In order to simplify equation (6) further, following definitions are introduced

$$\zeta = r/r_o \qquad (9)$$

$$S^* = S/S_o \qquad (10)$$

and $$S_d^* = \left(\int_{\zeta_i}^{\zeta_s} \frac{d\zeta}{S^*(\zeta)} \right)^{-1} \qquad (11)$$

Using these variables, and solving for the boundary conditions, expression (6) can be written as

$$dX/dt = [D_s \rho_P S_o/(\rho_R r_o)] S_d^* (\gamma_s^* - \gamma_i^*) \qquad (12)$$

The densities and initial size parameters are known. However, in order to calculate the solid state diffusivity, D_s, as a function of the conversion rate, values for γ_s^* and γ_i^* must also be available. In the absence of information concerning these quantities we will solve for D_s^*, defined as the product of the diffusivity, D_s, and the difference $\gamma_s^*-\gamma_i^*$.

The value of S_d^* is to be calculated from (11), with the use of a structural model (grain,...), and is only a function of the conversion. In this study, the overlapping grain model (Lindner & Simonsson, 1981) was used, and adapted (by allowing the initial grain radius, r_o, to vary with conversion), such that the external surface would correspond to the predictions of Ranade & Harrison (equation 2).

3.4.2. Lattice Diffusion.

With the present kinetic data for synthetic lime, the product layer thickness at which diffusion becomes dominating can be calculated to be 4.2 nm. Depending on the particle size, this thickness corresponds to a different conversion (48% for ro=0.01 μm; 3% for r_o=0.2 μm).

The value of D_s^* is seen to differ significantly between the synthetic lime and the single crystal results (Figure 16). For the synthetic lime, and under 3000ppm SO_2 and 5% O_2, the value is

$$D_s^* = 0.8\ 10^{-10} \exp(-39\ \text{kcal/mol}\ /RT) \qquad (13)$$

At 800°C, this yields $D_s^* = 8.5\ 10^{-19}\ m^2/s$, or $8.5\ 10^{-15}\ cm^2/s$.

In order to compare with literature results, the concentration gradient used in these other studies must be known. In the sulfation literature, the diffusivity is measured from the reaction rate, using the gas concentration for the calculation of the gradient. When these diffusivities are corrected for the approach taken here, Figure 17 is obtained. It thus appears that the solid state diffusivities measured with the synthetic lime correspond well with other literature studies. The diffusivities measured with single crystals and Iceland Spar are almost two orders of magnitude higher, however (Figure 16).

Kingery et al. (1976) provides a comprehensive review of the meaning of different solid state diffusivities. They publish data based on the concentration gradient of radioactive tracers. Based on this gradient, lattice, self-diffusion coefficients for simple oxides were found to vary several orders of magnitude, from 10^{-15} to $10^{-8}\ cm^2/s$, with activation energies ranging from 30 to 90 kcal/mol. These diffusivities can be related to the diffusivity of the vacancies, according to the same authors, by determining the equilibrium concentration of vacancies. Using the data provided, one finds that in KCl, this concentration, at 1073K, is $9.2*10^{-5}$ mol vacancies/mol. This number must be multiplied with the above diffusivities to obtain a value that can be compared with our D_s^*. The range becomes thus 10^{-19} to $10^{-12}\ cm^2/s$. Both diffusion coefficient and activation energy fall within the range expected for lattice diffusion.

3.4.3. Crystal Boundary Diffusion

This lattice diffusion, however, can only be observed in small particles

(< 1 μm). Larger particles exhibit a different, faster diffusion mechanism which is attributed to crystal boundary diffusion. The appearance of the $CaSO_4$ crystals on the product layer of the various samples (Figure 18) provide some insights as to the possible reason. The sulfate crystal boundaries in the product layer of the large single crystal can be identified by the raised edges, giving the crystals a dish-shape. The size of these crystals are often larger, but are in the same size range as the crystals found on the synthetic lime (0.5 to 1 μm), and larger than the dimensions of the primary particle of the synthetic lime.

Using these observations, it is postulated that the sulfate crystals formed on small particles quickly grow to a size that is larger than the initial CaO grains. They thus "swallow" the original grain, blocking off all easy access to the unreacted oxide. Figure 19 illustrates this qualitative description. When larger particles are employed, however, the sulfate crystals remain smaller than the underlying oxide. The boundaries between these crystals are highly disordered, and provide paths for faster diffusion. The dish-shape indicates that more material is deposited along these boundaries. Mess (1989) described the recarbonation of CaO single crystals in a similar way as limited by crystal boundary diffusion.

Evidence supporting the crystal boundary diffusion mechanism, is presented in Figure 20. It was obtained by measuring the sulfation rate of Iceland Spar at 800°C, using combination runs. A first sulfation was accomplished at various temperatures for different amounts of time, chosen such that the product layer would have the same thickness (3 and 11 minutes at 700 and 900°C, respectively). This first step created a product layer, upon which further sulfation was performed at 800°C. The rate was slower when the

preparation temperature was higher. Simultaneously, Figure 21 shows that for similar sulfation times, the sulfate crystal size increases with increasing temperature. This is evidence that the sulfation rate increases when the particle size decreases, in accordance with the proposed mechanism.

Crystal boundary diffusivity can be described as

$$D_{cb} = \ell/A \quad D' \tag{14}$$

where ℓ/A represents the crystal boundary length per unit area. This quantity is inversely proportional to the crystal diameter, d. The parameter D' represents the grain boundary diffusivity. Its dimensions are m^3/s (or cm^3/s). It can be considered to be the diffusivity through the disordered crystal boundary times the crystal boundary thickness. As this last quantity is unknown but assumed constant, we use D' as a dummy parameter that incorporates all unknown constants. Doing so, we can expect

$$D' = D_{cb} \quad d \tag{15}$$

to be a constant during conversion, in opposition to the value of D_{cb}, that decreases almost an order of magnitude at early time, as shown in Figure 16. The inaccuracy in the crystal size measurements on SEM pictures results in considerable scatter in the value of D' (Figure 22). However, it eliminated the change in diffusivity with time, observed in Figure 16.

Using expression (15), it was possible to obtain a value, shown in Arrhenius form in Figure 23.

$$D' = 1.4\ 10^{-16} \quad \exp\ (-28\ \text{kcal/mol} \quad /RT)\ (m^3/s) \tag{16}$$

The activation energy for crystal boundary diffusion is typically much lower than for lattice diffusion (Kingery et al., 1976), in accordance with what is observed here.

3.4.4 Diffusing Species

Even though it was not possible to obtain information on the *rate-limiting* species, use was made of a combination run to test whether the $CaSO_4$ was formed on top of the product layer, or at the solid-solid interface. If the sulfate is formed at the interface, the sulfur species must diffuse through the product layer, probably in its sulfate form, as this ion is covalently bound and thus unlikely to decompose. If the product is formed on top of the layer, both Ca^{++} and O^{--} are diffusing out, towards the gas phase.

Calcium sulfate does not react with CO_2, as the sulfate is more stable than the carbonate. However, if CaO is present on the outer surface, CO_2 can react and a weight increase can be registered on the TGA recorder. Hence, in the first step of the combination run, the sample was sulfated to the point where product layer diffusion is rate-limiting. At that point, the sulfur containing gas is replaced by CO_2, and the weight is recorded. The synthetic lime exhibited formation of carbonate, as testified in Figure 24 by the weight loss due to its decomposition, when CO_2 is replaced by an inert gas (He). The larger, single crystals for which grain boundary diffusion is rate-controlling, showed no measurable reaction with CO_2 when subjected to a similar exposure history, indicating the absence of CaO on the outer surface. For this material, the sulfur species is diffusing via the crystal boundaries towards the interface to react with CaO.

These observations are consistent with the expectation that where lattice diffusion occurs, the smallest species will diffuse orders of magnitude faster than the larger ones. In the crystal boundaries, where the concentration of defects is much larger, the larger SO_4^{--} units diffuse much easier.

3.4.4. Dependence on SO_2 partial pressure

The dependence of the rate on the SO_2 concentration in this regime was determined as well. The order of 0.6, measured at low conversion, decreased to 0.25 at high conversion with synthetic limes, and to 0.2 with single crystals and Iceland Spar. An explanation for this phenomenon is probably to be found in the dependence of the thermodynamic equilibrium, γ_S^*, on the partial pressure.

Theories of this sort exist and have been investigated in other circumstances (Fröger, 1964). No further investigation on this subject was performed in this work.

3.5. Use of the Regime Map

The purpose of the above discussion was to provide arguments for the existence, and for the conditions needed for the various regimes. The most important parameters found to determine what regime is controlling are the grain size and the conversion. Hence, the map shown in Figure 25 is proposed. It is applicable at 800°C and 3000ppm SO_2. When temperature and gas concentrations change, the kinetic parameters change and the curves will move accordingly.

The boundary between kinetic and solid state diffusion controlled regimes is obtained by assuming a structural model (overlapping spherical grains in this case), and calculating the conversion at which the product layer reaches the critical thickness as a function of grain size.

The boundary between the two solid state diffusion regimes, however, is not as easy to determine. The reason is that it depends on the crystal sizes in the product layer, for which no unambiguous size prediction can be made.

Nevertheless, a few points of reference can be used. When the grain size is smaller than the smallest crystal size observed, the crystal cannot stand on its own and will incorporate the grains, thus eliminating all high diffusion paths. The smallest crystal size ever observed was about 0.1 μm in diameter. However, these small crystals grow fast until they reach an asymptotic value. The parameter needed here is time rather than conversion; qualitatively, using the observed time-conversion particle size relationship, the lower dashed curve in the regime map, Figure 25 can be drawn.

The higher end of this boundary is even more qualitative. We know that the synthetic limes, whose grain size lie between 0.2 and 0.4 μm exhibits lattice diffusion exclusively, and at the other hand, that small (1-2 μm) Iceland Spar samples provided large diffusivities, indicative of crystal boundary diffusion. Thus, the upper dashed line, rising similarly as the lower line must be drawn in between these extremes.

As a grain sulfates, it moves on an horizontal line in the regime map. The submicron ash (d=0.015 μm), with the highest surface area of all samples investigated, will be in the kinetic regime until over 50 % conversion. The synthetic lime (0.2-0.4 μm) still allows us to measure a kinetic regime, but will rapidly be controlled by lattice diffusion. All grains larger than 1 μm will only react according to the crystal boundary diffusion mechanism.

Porous materials that exhibit pore filling, as most natural limes, behave differently before and after pore filling. As long as the internal grains (whose size can be determined from the internal specific surface area) can react independently, they can be regarded as independent particles. The kinetic and subsequent lattice diffusion mechanism will dominate. This is why most authors observed the slower, lattice diffusion rate. When pore filling

occurs, however, the individual grains cease to exist as independent units, and the particle size becomes important. Soon, crystal boundary diffusion takes over the sulfation process.

At that point, only the external surface is available for reaction, such that the overall rate is dramatically reduced. The time needed for further conversion depends on the sulfate crystal size in the product layer. Figure 26 presents the time needed to react from 40% (when pore filling occurs) to 60%, assuming lattice diffusion at the one hand, and crystal boundary diffusion, with various crystal sizes, at the other hand. It is expected that very small particles, less than 1 μm in diameter, will exhibit lattice diffusion only, and thus react slower than larger particles that can reach the crystal boundary diffusion regime. When still larger particles are used, the crystals have time to grow, which results in a reduction in the diffusivity. For particles larger than 0.5 μm diameter, an optimal size, where time for full sulfation is shortest, is therefore predicted.

5. Conclusion

The object of this work is to provide a mechanistic understanding of the lime sulfation process.

Although the chemical ($CaSO_4$) and physical (solid crystals) composition of the product layer is known, the traditional description of the product layer diffusion mechanism assumes a homogeneous product layer, and a driving force proportional to the gas concentration of SO_2 (as if gaseous diffusion were occurring). Such a model is unable to describe diffusivity changes during the sulfation process, or large differences in diffusivity among different

samples. The model suggested in this work allows for the more realistic case of ionic diffusion through the product layer. The product layer structure was found to, in some cases, produce high diffusivity paths that affect the conversion behavior.

Model stones were designed in order to provide kinetic information. Measurements of the surface area with sulfation time indicated that a sintering process occurred, thus explaining the faster decrease in rate than predicted by the traditional structural models.

Three rate-controlling regimes were postulated (Figure 23.) At early conversion, the rate is controlled by the kinetic, or surface reaction rate. When conversion increases, the transition depends on the particle size-product layer diffusion becomes important. If the grain size is smaller than 1 μm, lattice diffusion takes over. This occurs when the sulfate crystals become so large that they 'swallow' the original grain. If the original grain is large enough the sulfate crystals in the product layer cannot surround the CaO, and the crystal boundaries provide fast diffusion paths for further reaction.

The rate dependence on SO_2 partial pressure was also examined. In the early stage, an order of 0.52 was found, and in the product layer diffusion regime, the order decreased to 0.2 (for crystal boundary diffusion) or 0.25 (for bulk diffusion).

6. References

Bardakci,T.: "Diffusional Study of the Reaction of Sulfur Dioxide with Reactive Porous Matrices" Thermochim.Acta, 76, 287 (1984)

Bhatia S.K. and D. Perlmutter:"The Effect of Pore Structure on Fluid-Solid Reactions: Application to the SO_2-Limestone Reaction", AIChE J. 27, 226 (1981a)

Borgwardt,R.H.: "Kinetics of the Reaction of $SO_2$with Calcined Limestone" Env. Sci. and Techn., 4, 59 (1970)

Borgwardt,R.H.and R.Harvey: "Properties of Carbonate Rocks Related to SO_2 Reactivity", Env. Sci. and Tech., 6, 4, p350 (1972)

Borgwardt,R., N. Roache & K. Bruce: "Method for Variation of Grain Size in Studies of Gas-Solid Reactions Involving CaO" Ind. Eng. Chem. Fund., 25, 165 (1986b)

Cabrera,N. & N.F.Mott: "Theory of the Oxidation of Metals", Report on Progress in Physics, 12, 163 (1949)

Ferguson,O.L. & E.F. Rissman: "An Infrared Kinetic Study of Mechanisms Involved in the Dry Limestone SO_2 removal Process": Proceedings of the 2nd International Clean Air Congress, by H.M. Englund & W.T Berry (editors), Academic Press, NY, 1971

Fischer,H.C.: "Calcination of Calcite: I, Effect of Heating Rate and Temperature on Bulk Density of Calcium Oxide" J. Am. Cer. Soc., 38, 7, 245 (1953)

Floess,J., PhD Thesis, MIT, 1985

Fröger, F.A.: "Chemistry of Imperfect Crystals", North Holland Publishing Coo.-Amsterdam; J.Wiley & Sons, NY, 1964

Glasson, D.R.: "Reactivity of Lime and Related Oxides. I Production of Calcium Oxide" J. Appl. Chem., 8, 793 (1958)

Gopalakrishnan,R. & M.S. Seehra: "Kinetics of High-Temperature Reaction of SO_2 with CaO Particles using Gas-Phase Fourier Transform Infrared Spectroscopy" Energy & Fuels, 4, 226 (1990)

Hartman,M. and O. Trnka: "Influence of the Temperature on the Reactivity of Limestone Particles with Sulfur Dioxide", Chem. Eng. Sci., 35, 1189 (1980)

Hartman,M. & J. Pata: "Texture of a Limestone Calcine and its Reactivity with Sulphur Dioxide" Collection Czechoslov. Chem. Commun., 44, 2465 (1979)

Hartman, M. & R.W. Coughlin: "Reaction of Sulfur Dioxide with Limestone and the Influence of Pore Structure" Ind. Eng. Chem., Process Des. Develop.,13, 248 (1974)

Hartman,M. & R. Coughlin: "Reaction of Sulfur Dioxide with Limestone and the Grain Model" AIChE. J. 22, 490 (1976)

Jost,W : "Diffusion in Solids, Liquids and Gases" Academic Press, New York, 1952

Kingery,W.D., Bowen & Uhlman: "Introduction to Ceramics", John Wiley & Sons, 1976

Kronenberg,A.K., R.A. Yund, B.J.Giletti: "Carbon and Oxygen diffusion in Calcite; effects of Mn content and P_{H2O}" Phys. Chem. Min., 11, 101 (1984)

Lindner,B. & D. Simonsson: "Comparison of Structural Models for Gas-Solid Reactions Undergoing Structural Changes" Chem. Eng. Sci., 36, 9 1519 (1981)

Low,M.J.D., A.J.Goodsel, N.Takezawa: "Reactions of Gaseous Pollutants with Solids: Infrared Study of the Sorption of SO_2 on CaO" Env. Sci. & Tech., 5, 12, 1191 (1971)

Marcilly,L., P. Courty and B. Delmon: "Preparation of Highly Mixed Oxide Solutions by Pyrolysis of Amorphous Organic Precursors", J. Am. Cer. Soc., 53, 1, p56 (1970)

Marsh,D.W. & D.L.Ulrichson: "Rate and Diffusional Study of the Reaction of Calcium Oxide with Sulfur Dioxide" Chem. Eng. Sci., 40, 3, 423 (1985)

Mess,D.: "Product Layer Diffusion in the Carbonation of Calcium Oxide", PhD Thesis, MIT, 1989

Milne,C.R., PhD Thesis, Univ. of Utah, 1988

Ramachandran,P.A. & L.K. Doraswamy: "Modeling of Noncatalytic Gas-Solid Reactions" AIChE. J., 28, No6, 881 (1982)

Ranade,P.V. & D.P. Harrison: "The Grain Model Applied to Porous Solids with Varying Structural Properties" Chem. Eng. Sci., 34, 427 (1979)

Shewmon, P.G.: "Diffusion in Solids", William Book Co., 1983

Siriwardane,R.V.: "Effect of O_2 on the Interaction of SO_2 with CaO (100), Iron Deposited on CaO (100), and Sodium Deposited on CaO (100)" J. of Coll. and Int. Sci., 116, No2, 463 (1987)

Staudinger, G. & H. Schröfelbauer: "Laboratory Tests, Field Trials and Application of Furnace Limestone Injection in Austria", Paper presented at the first Joint Symposium on Dry SO_2 and Simultaneous SO_2/NOx Control Technologies, San Diego, nov 1984

Szekely,J., J. Evans and H.Y. Sohn: "Gas Solid Reactions", Academic Press, New York, 1976

Van Houte,G. & B. Delmon: "Kinetics of the Reaction of $CaCO_3$ with SO_2 and O_2 below 650°C", J. of The Chem. Soc., Faraday Transactions I, 75, 1593 (1979)

Wen,C.Y. & M. Ishida: "Reaction Rate of Sulfur Dioxide with Particles Containing Calcium Oxide", Env. Sci. & Tech., 7, 703 (1973)

TABLE 1

Types of Materials used in this Study

	Iceland Spar (Calcined)	Submicron Ash	CaO Single Crystals	Synthetic Lime
Particle Size	15-20 μm	0.015 $\mu m^{\#}$	10-15 μm	100-150 μm
Surface Area (S_o)	30 m^2/g	120 $m^2/g^{\#}$	0.2 $m^2/g^{@}$	5 m^2/g
Porosity	54 %	0 %	0 %	90-95 %
Thiele Modulus	0.9	0*	0*	0.2
Effectiveness Factor	0.7	1.0	1.0	0.97

NOTE: #: Estimated from TEM pictures

@: Estimated from SEM pictures

*: For non-porous material, the Thiele modulus is zero because no reaction occurs in the bulk

Table 2. Description of Synthetic Lime Samples

Sample ID	ratio $\frac{\text{citric acid}}{Ca(NO_3)_2}$	Calcination Temperature ($^{\circ}C$)	Calcination Time (hours)	BET Surface Area (m^2/g)	Pore Volume (cm^3/g)
R	1:1	1100	3	5.5	4.2
R1088	1:1	1000	4	6.3	4.4
R289	1:1	1000	3.5	3.9	4.8
R489	1:1	1100	6	4.0	4.6
R1189	1:1	1100	3	4.9	5.2
L	1:1	1100	8	3.3	3.3
L1088	1:1	1000	8	5.3	3.5
D	2:1	1100	3	5.6	2.9
D1088	2:1	1000	4	5.4	2.5

(aggregate size = 50-150 μm)

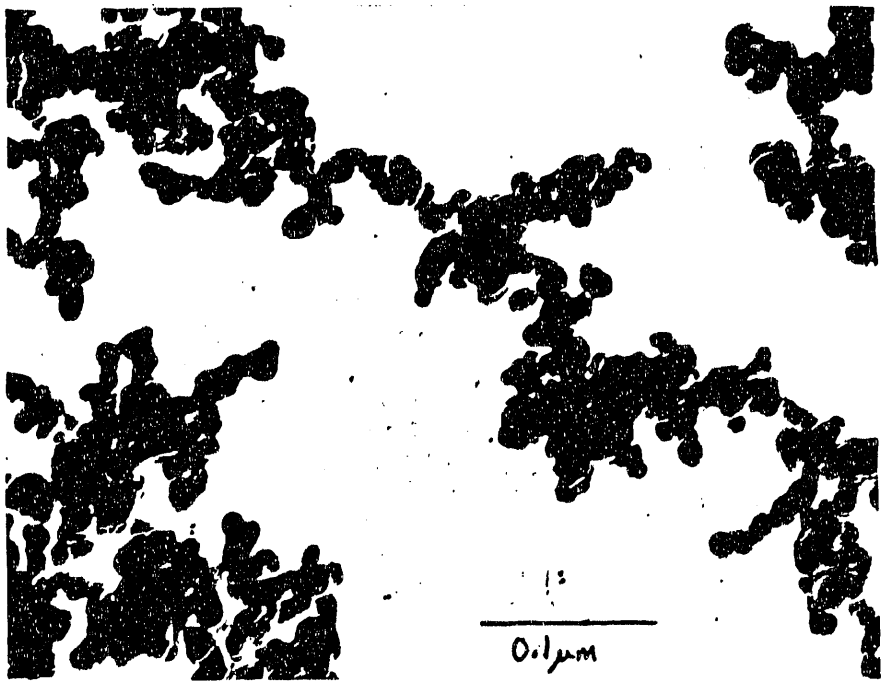

Figure 1. TEM picture of Submicron Ash

(a)

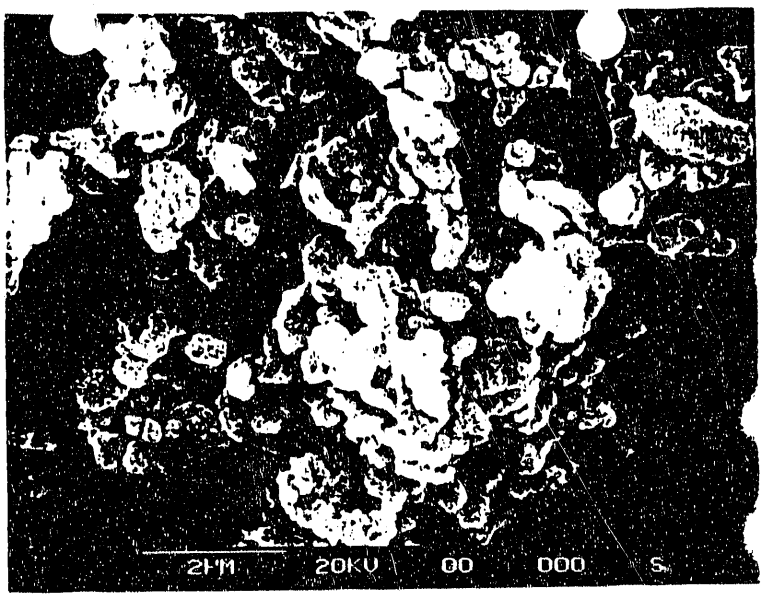

(b)

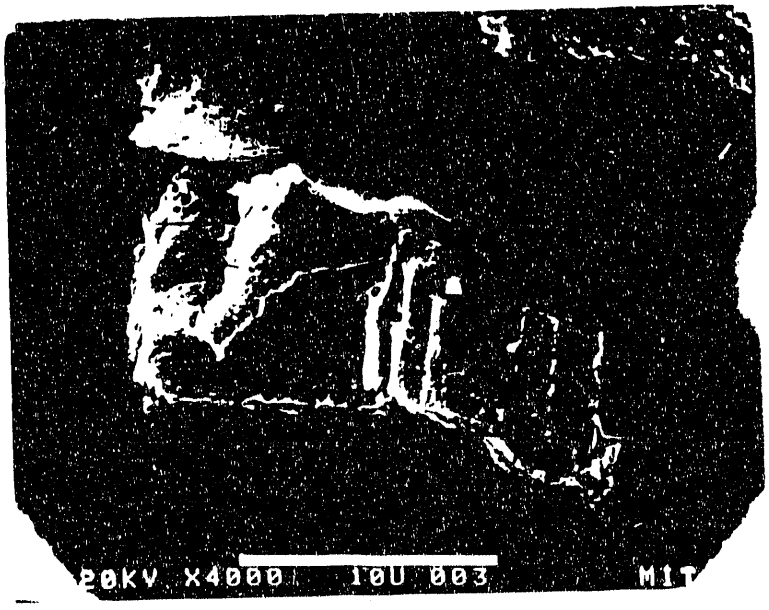

(c)

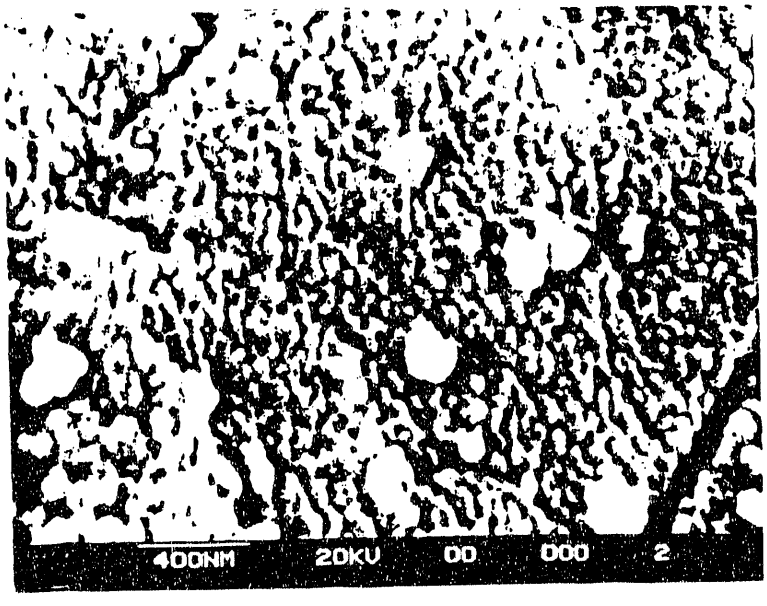

Figure 2. Microscopic Aspect of the Various CaO Samples Used:
(a): Synthetic Lime; (b) Single CaO Crystals; (c): Calcined Iceland Spar

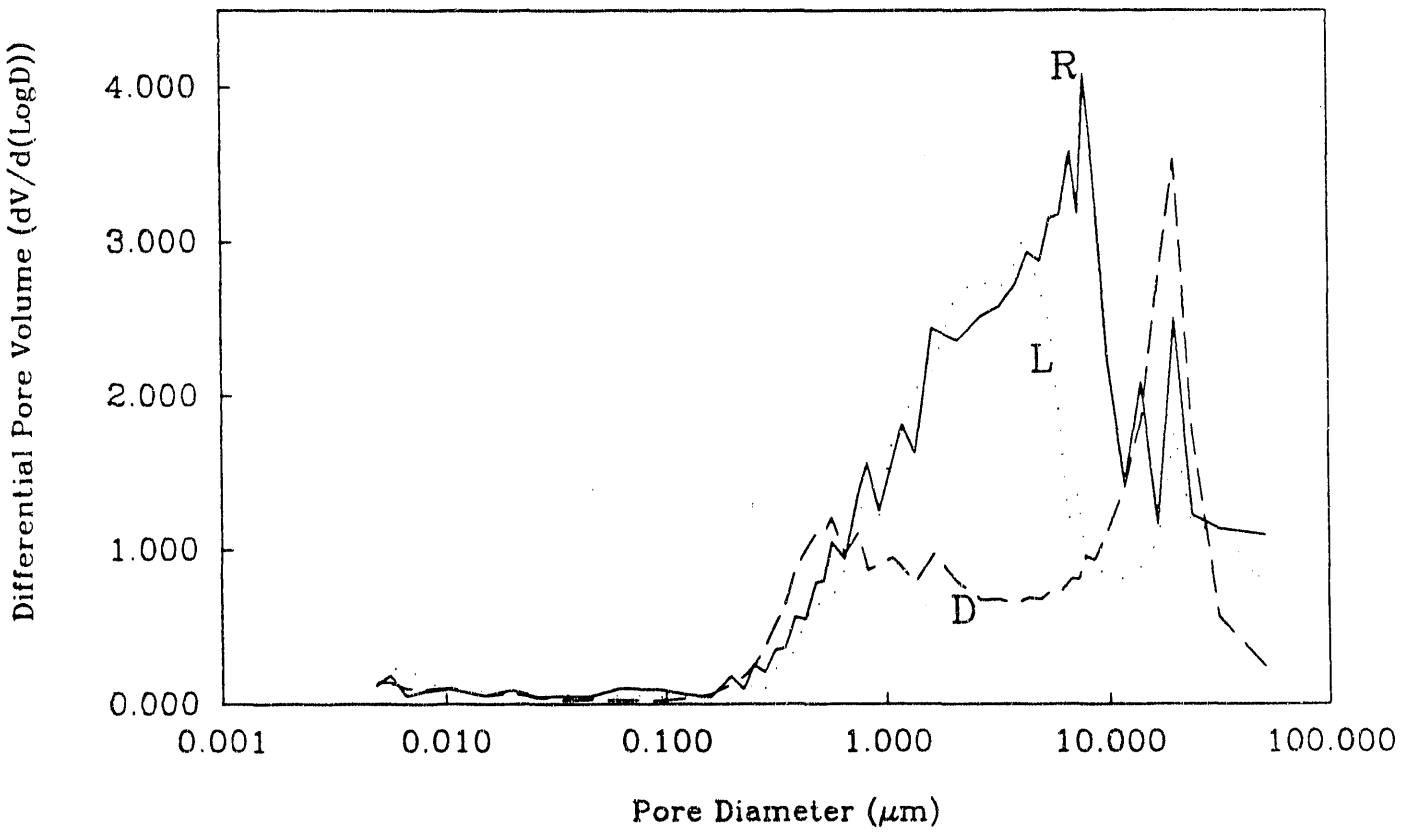

Figure 3. Pore Size Distribution of Synthetic Limes, Using Different Preparations: R and L have equimolar amounts of Ca and Citric Acid; R is Calcined at 1000°C for 3 hours; L for 8 hours. D is calcined for 3 hours, but has twice the amount of Citric Acid (see Table 2). Particle Size 50-150 μm.

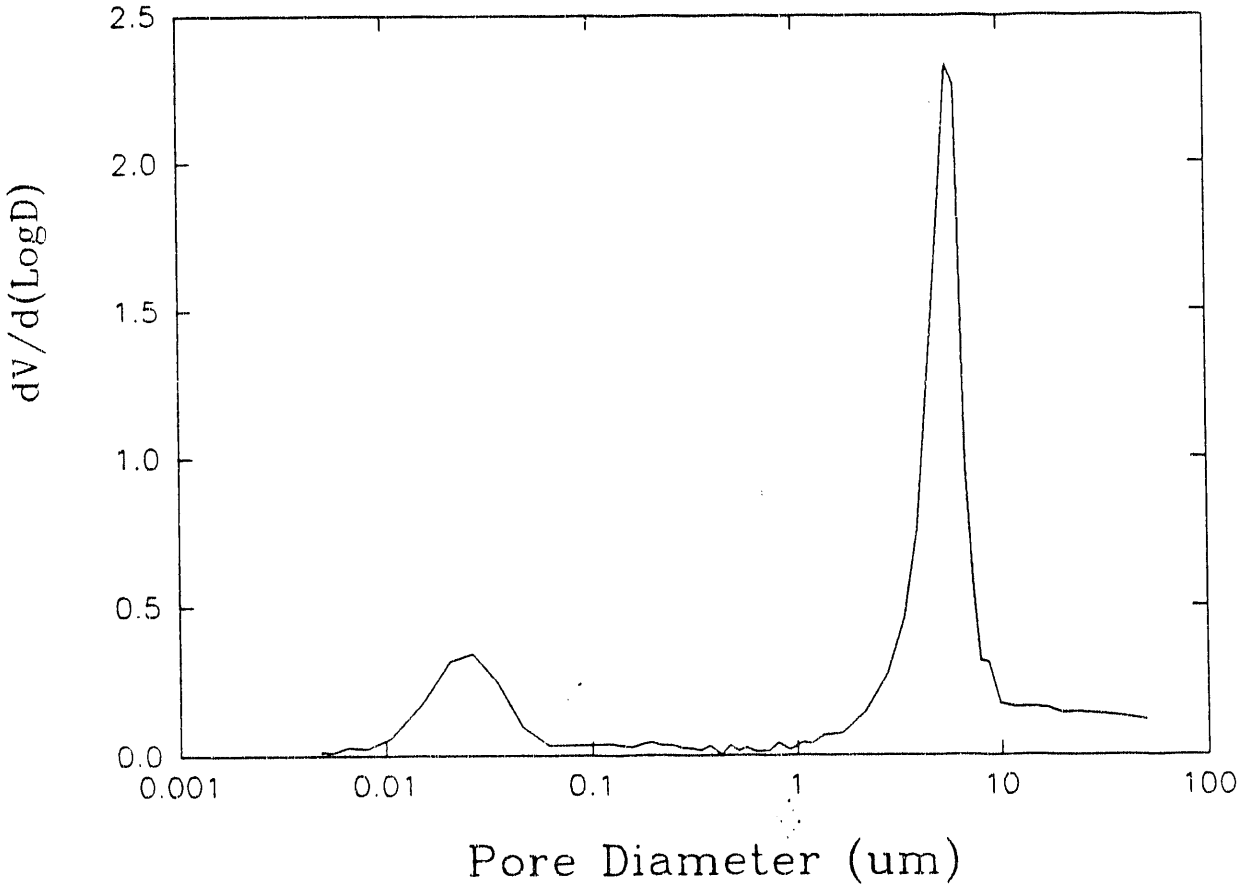

Figure 4. Pore Size Distribution of Iceland Spar, Calcined in a Helium Atmosphere, with a Heating Rate of 40°C/min. Particle Size 10-15 μm.

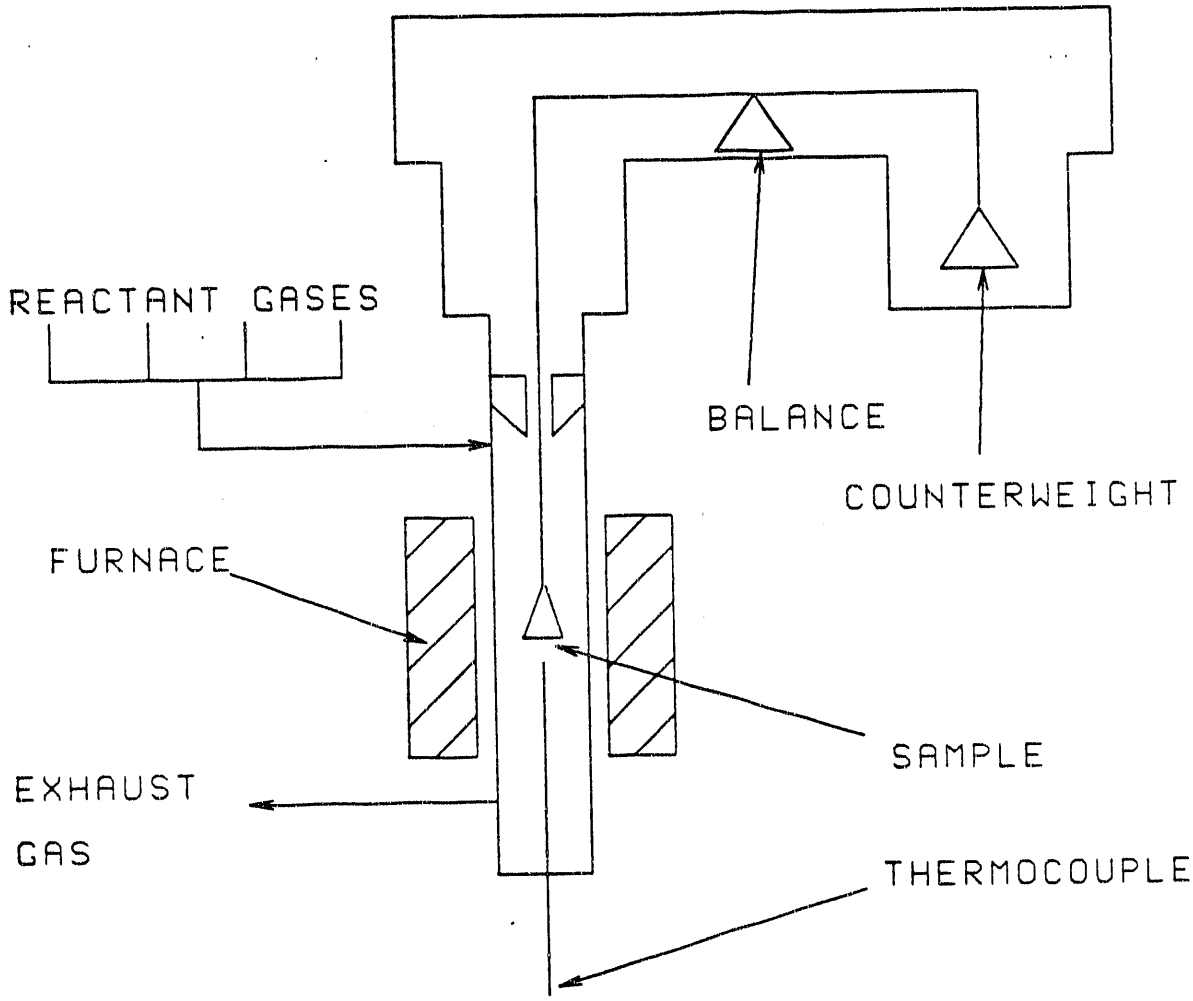

Figure 5. Sketch of the Thermogravimetric Analyzer

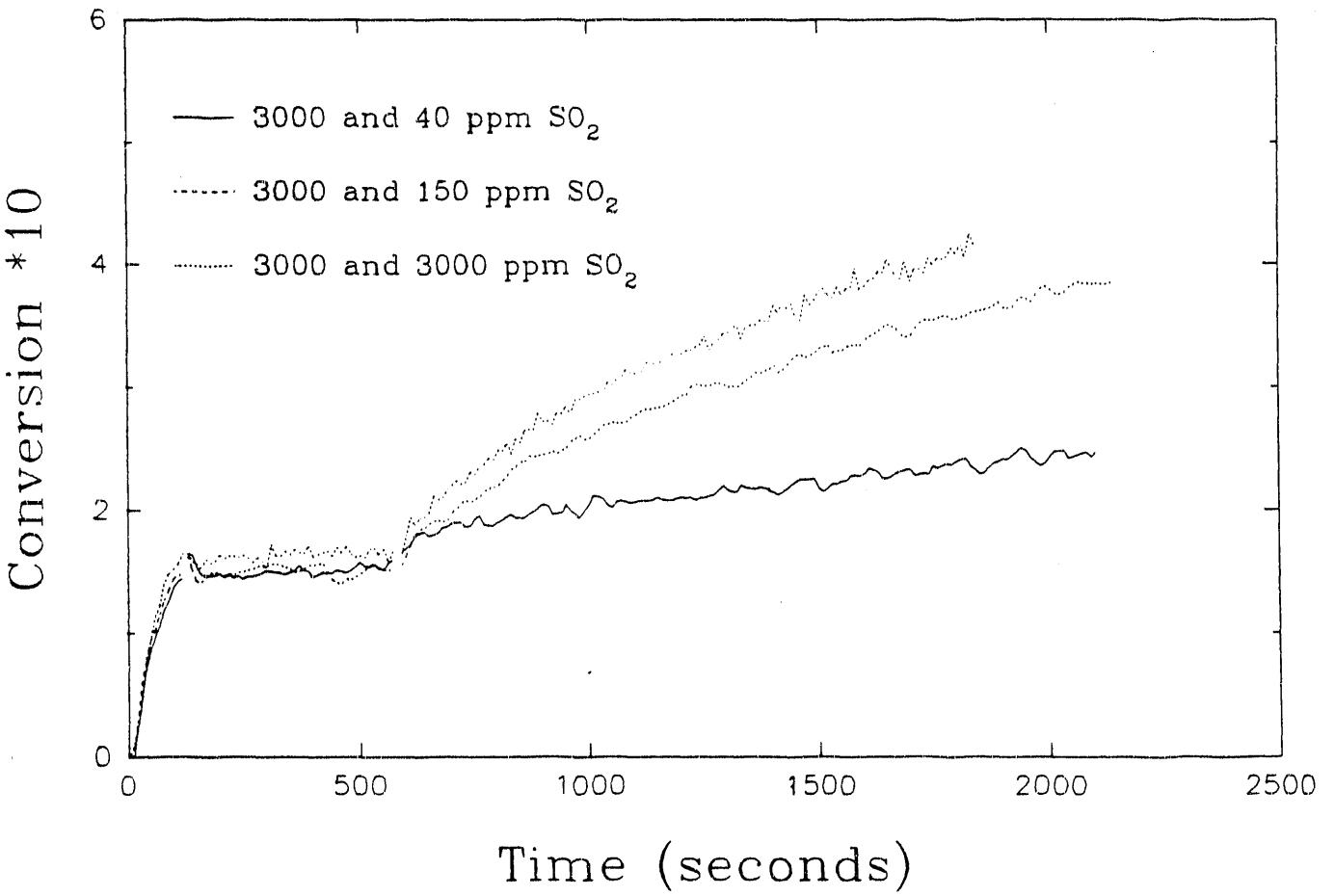

Figure 6. Example of Combination Run: Change of SO_2 concentration on Synthetic Lime, at 800°C

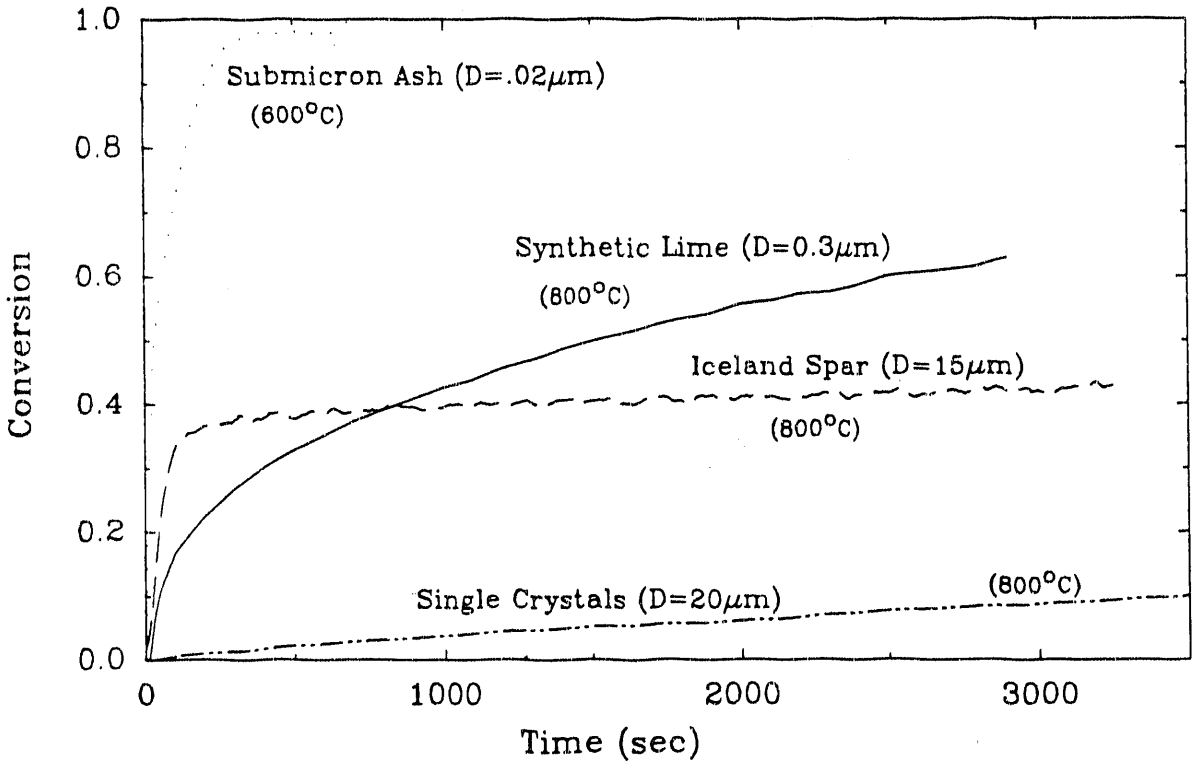

Figure 7. Conversion Behavior of Different Samples (3000ppm SO_2 and 5 % O_2)

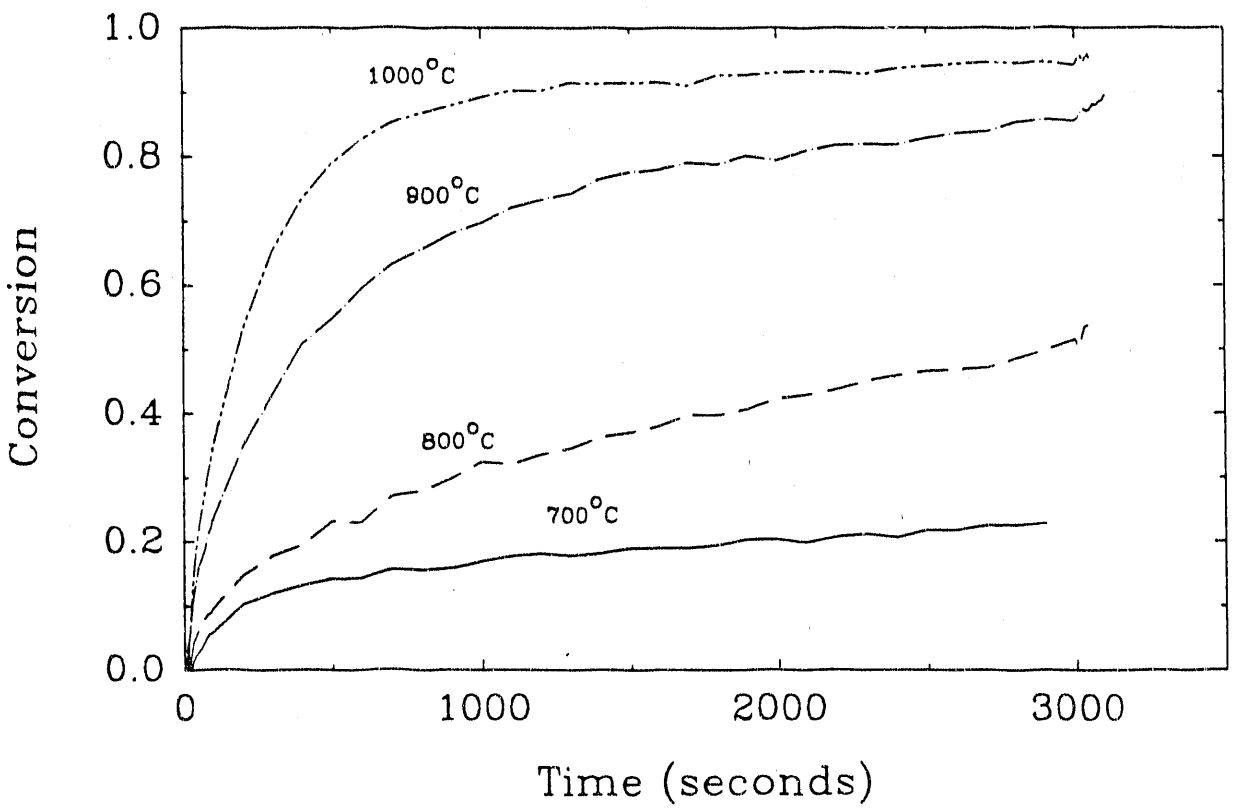

Figure 8. Conversion Behavior of Synthetic Lime, under 3000ppm SO_2 and 5% O_2 (Sample R489)

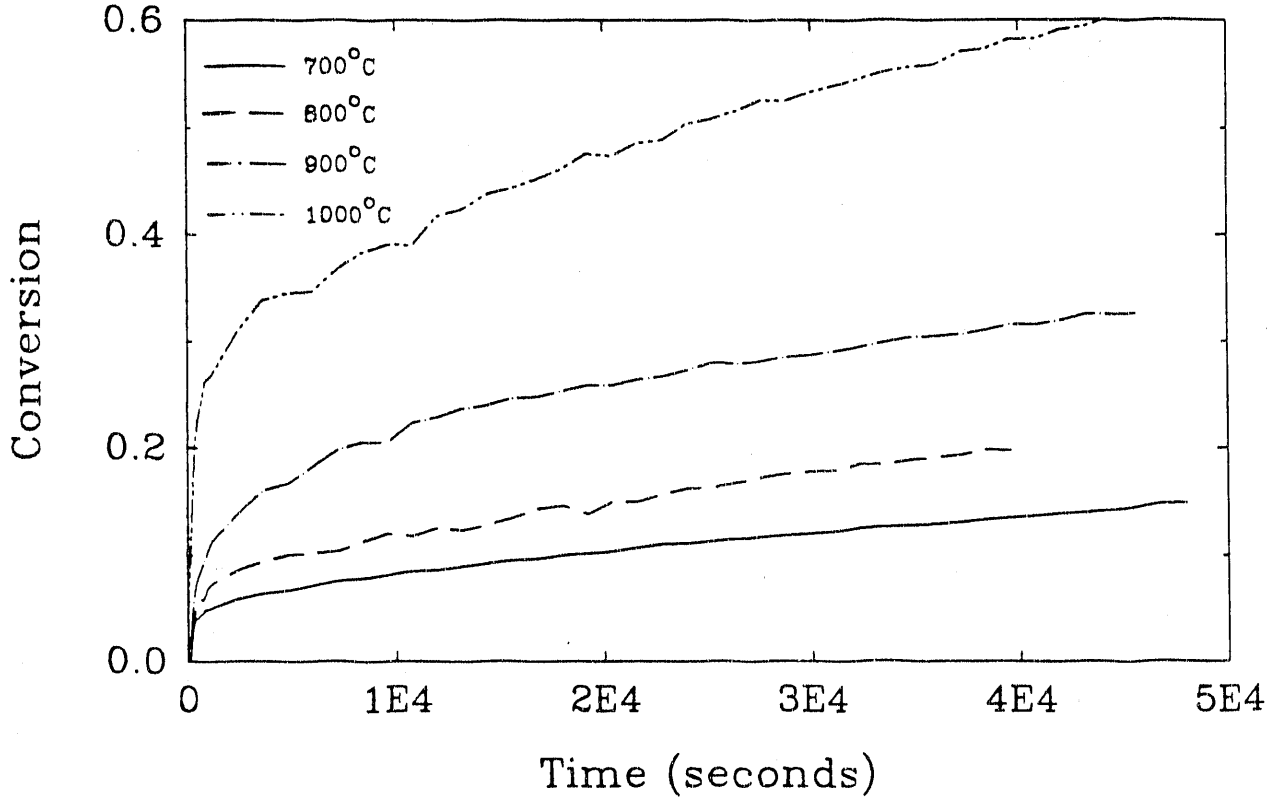

Figure 9. Conversion Behavior of Single Crystals, under 3000ppm SO_2 and 5% O_2

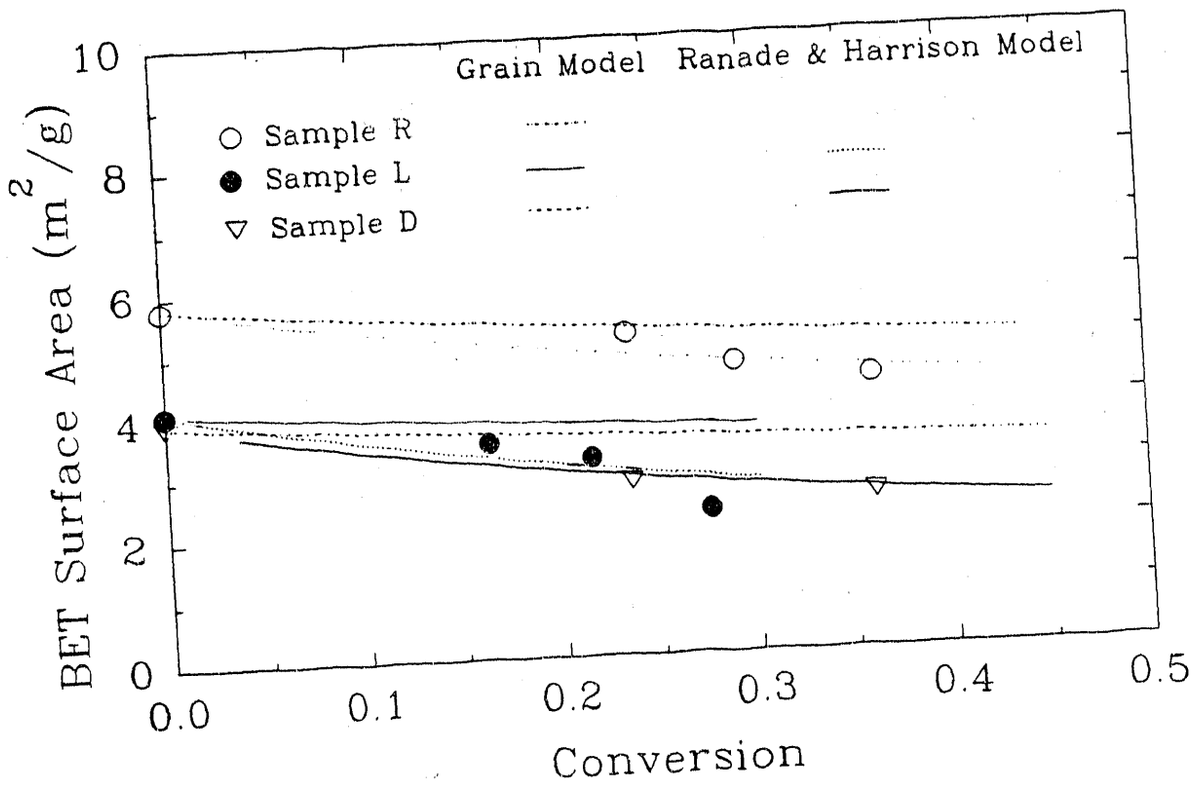

Figure 10. Surface Area Evolution During Sulfation, for three Synthetic Limes, Compared with the Simple Grain Model Predictions, and the Model of Ranade & Harrison (1979)

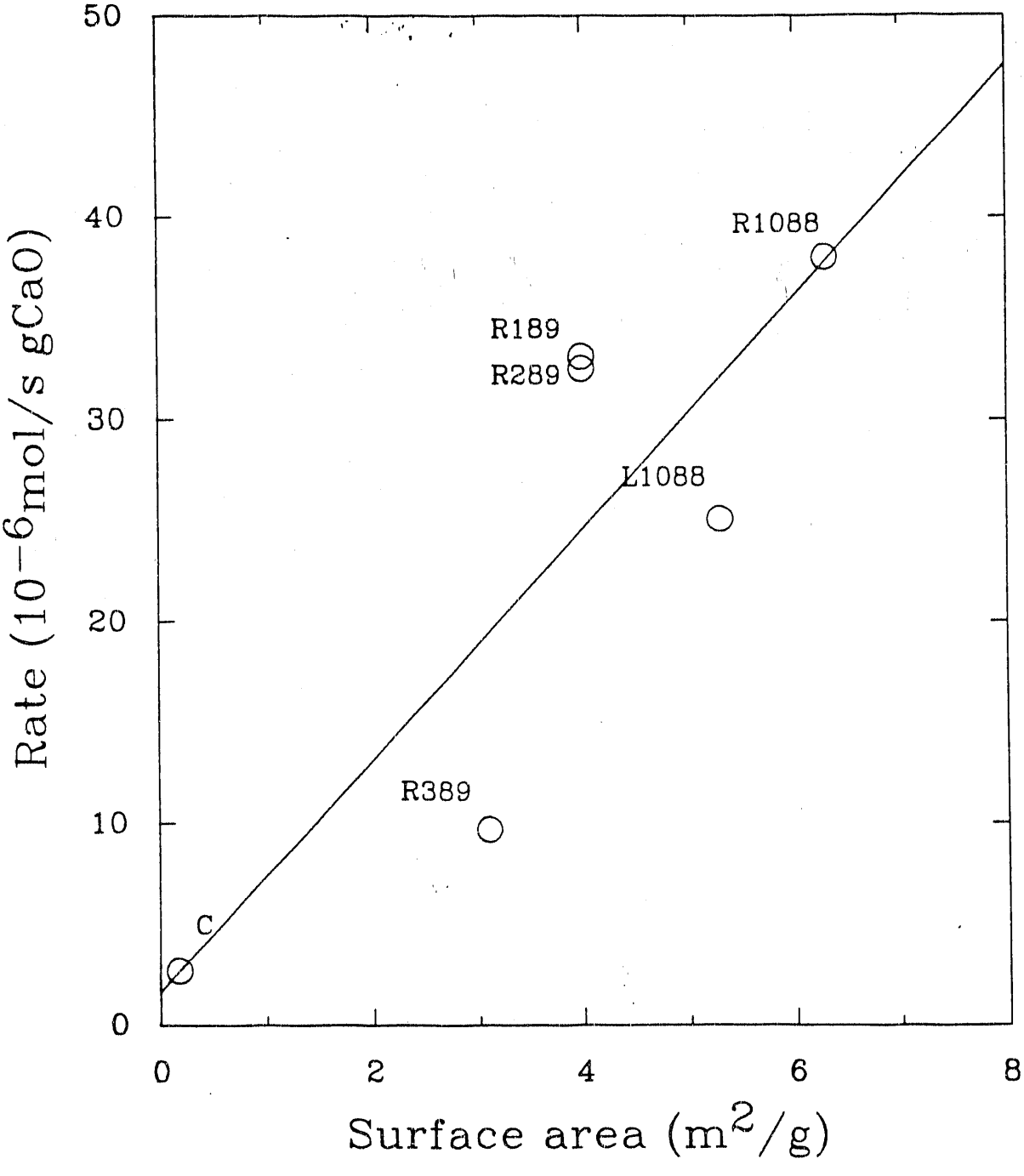

Figure 11. Dependence of the Initial Rate on the Surface Area. C stands for Single Crystals; the other labels designate Synthetic Limes (see Table 2)

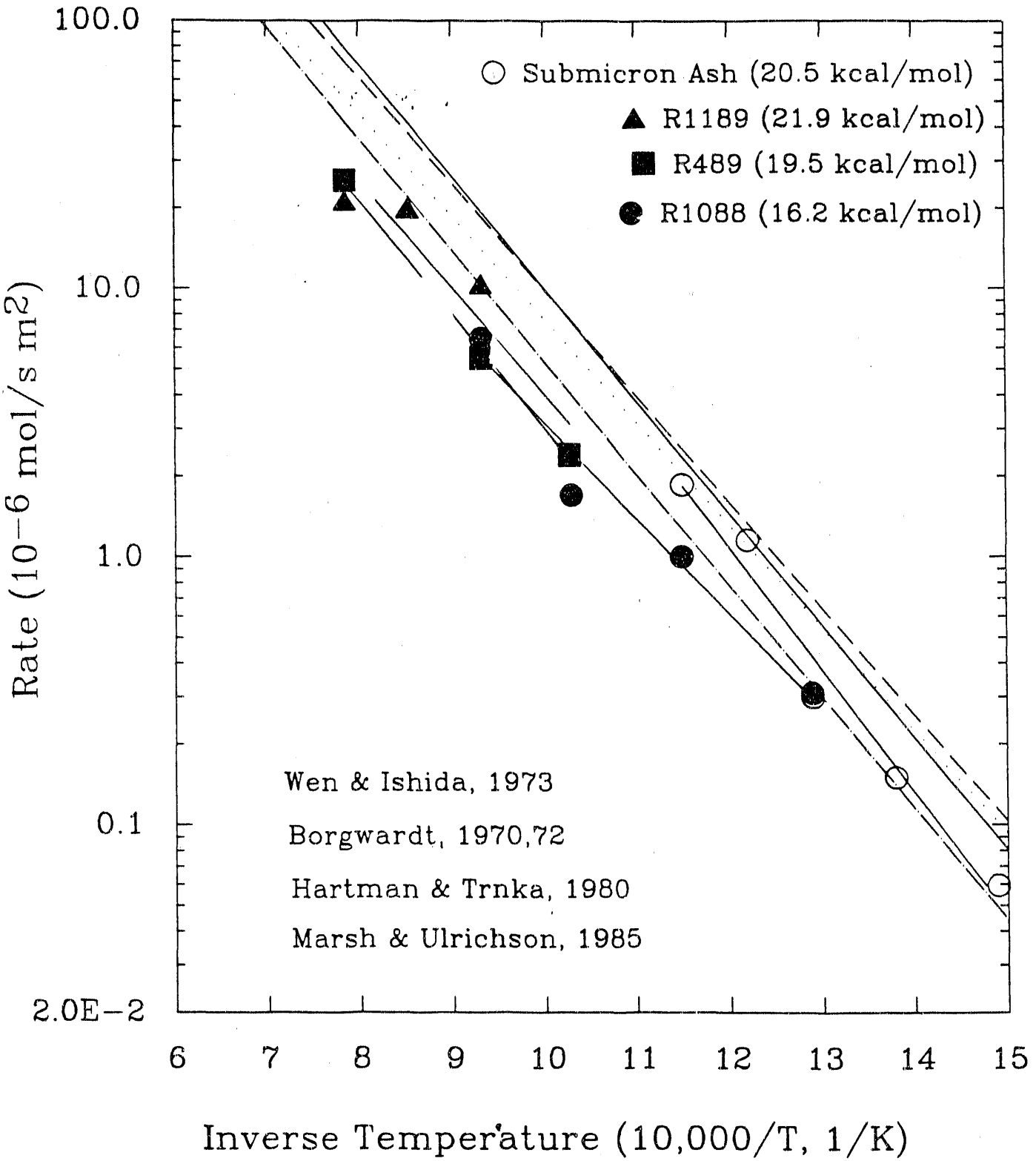

Figure 12. Arrhenius Plot for the Initial Rate, Comparing Results of Submicron Ash and Synthetic Limes with Literature (3000ppm SO_2; 5% O_2)

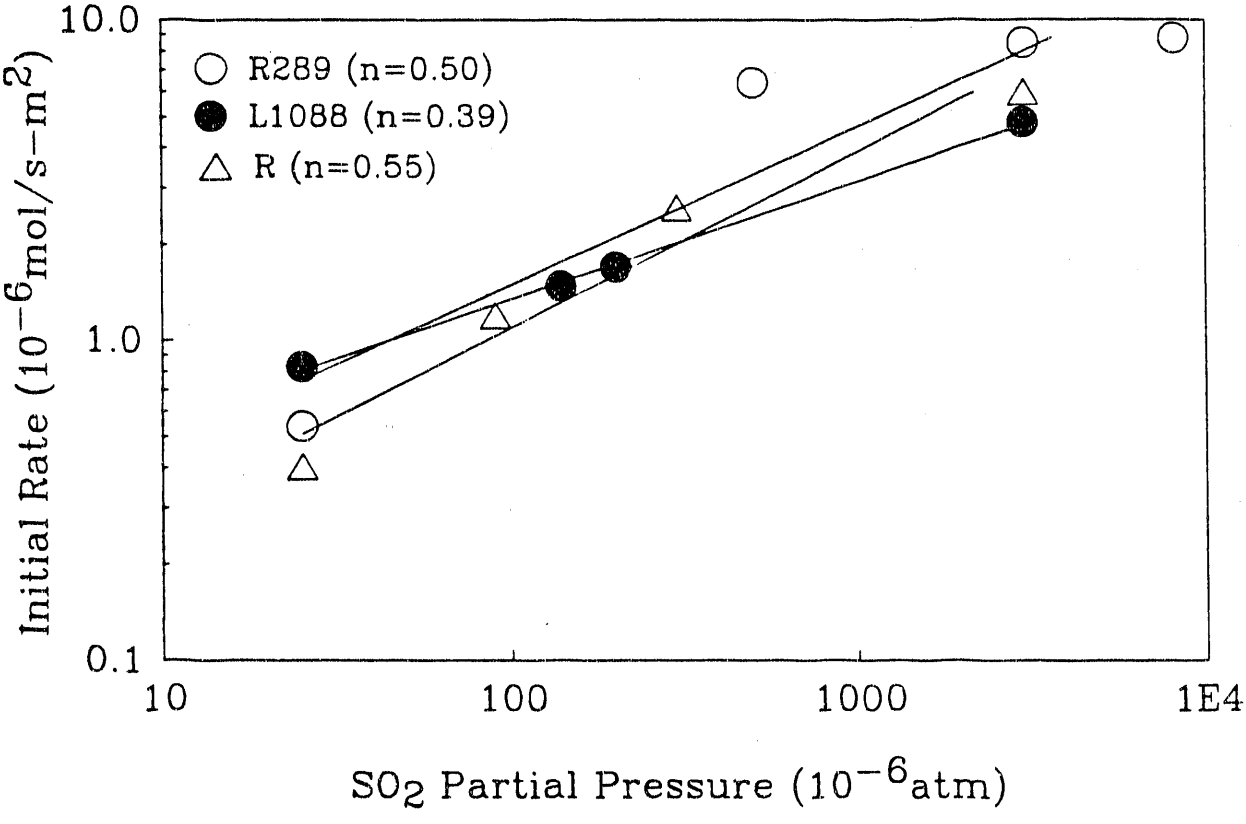

Figure 13. Order of Initial Rate on SO_2 Partial Pressure, at 800°C, and with 5% O_2

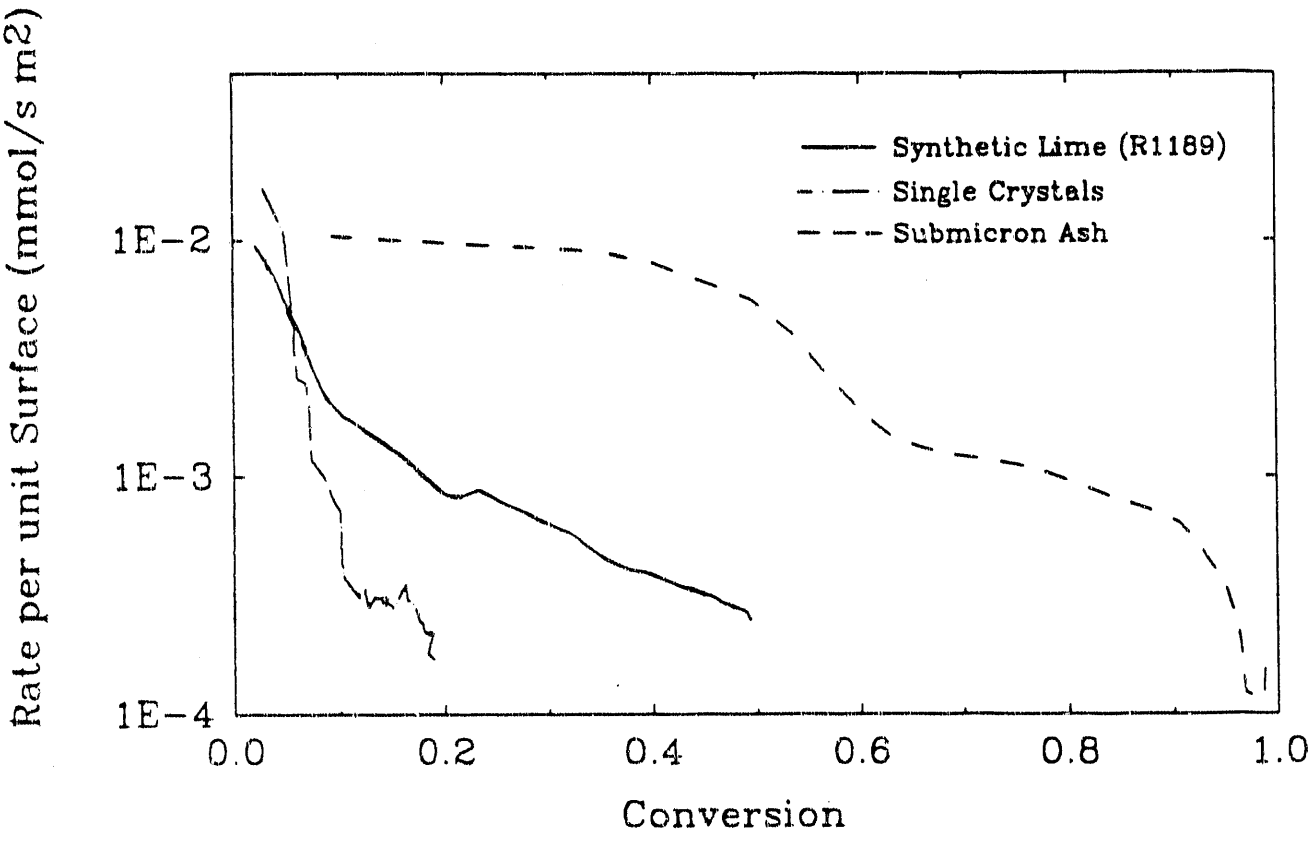

Figure 14. Rate per Unit Surface Area for Different Samples

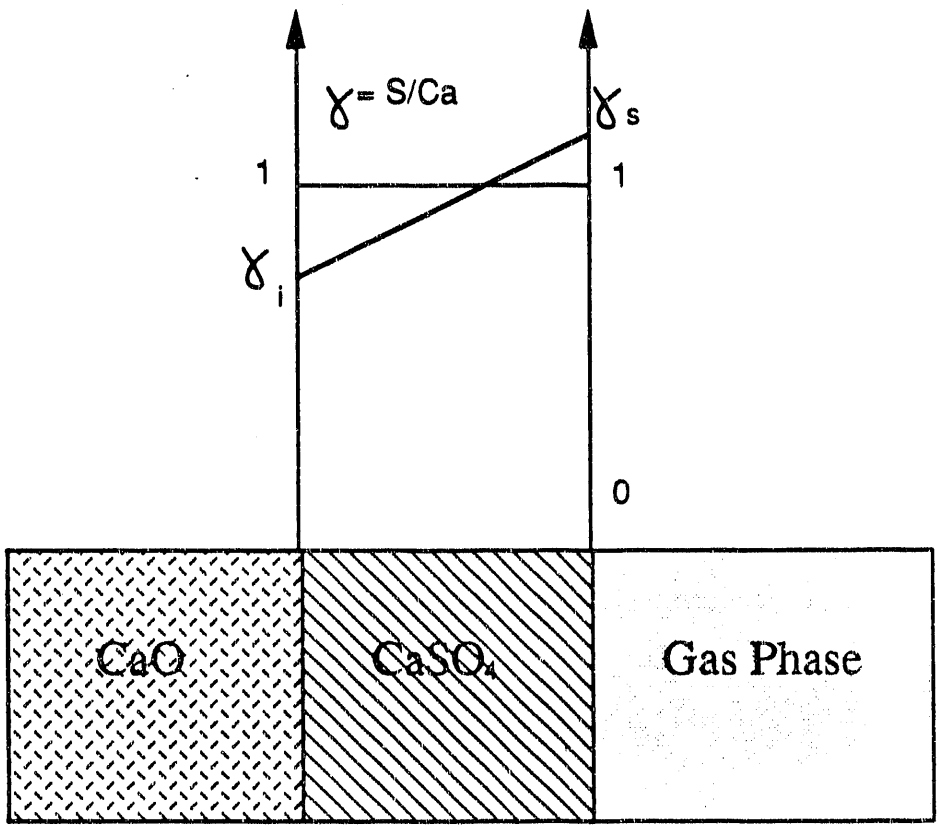

Figure 15. Illustration of the Definition of γ

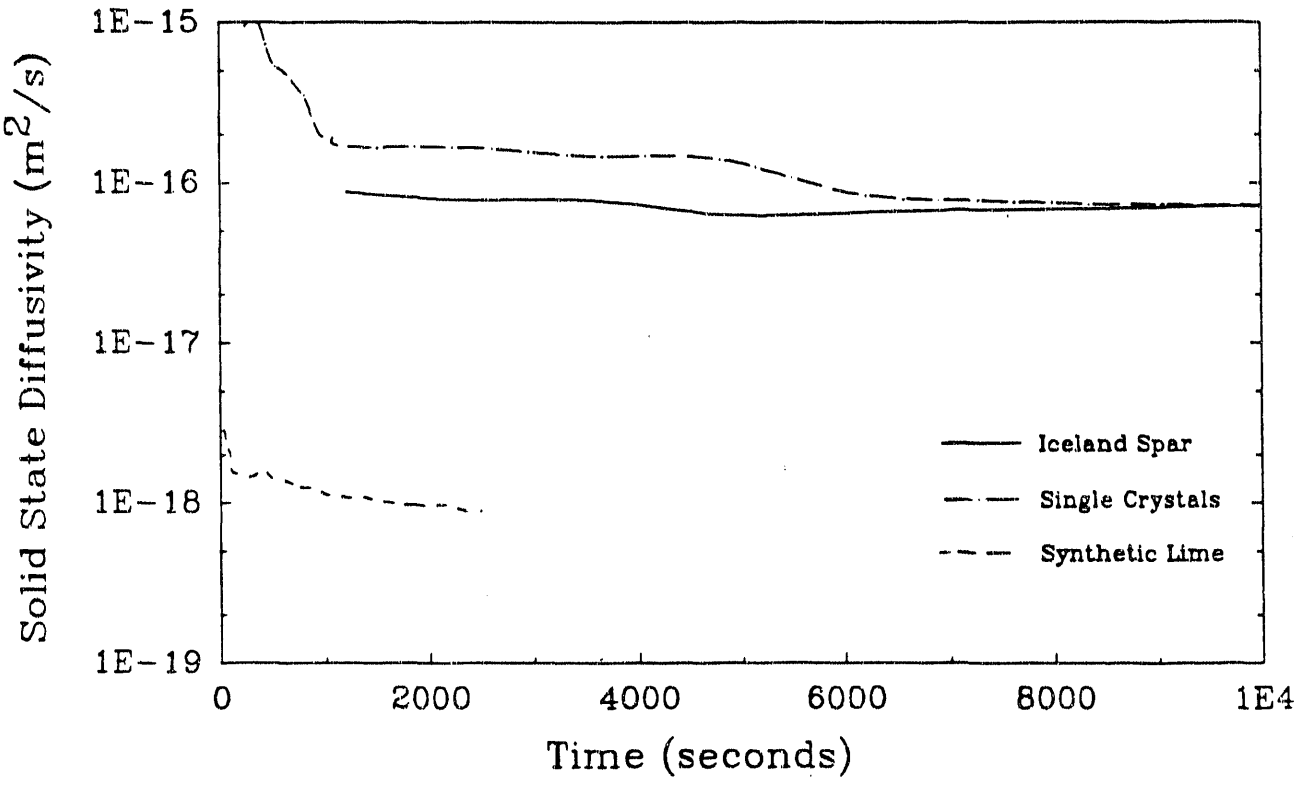

Figure 16. Solid State Diffusivity Behavior with time of the Synthetic Limes, the Iceland Spar and Single Crystals

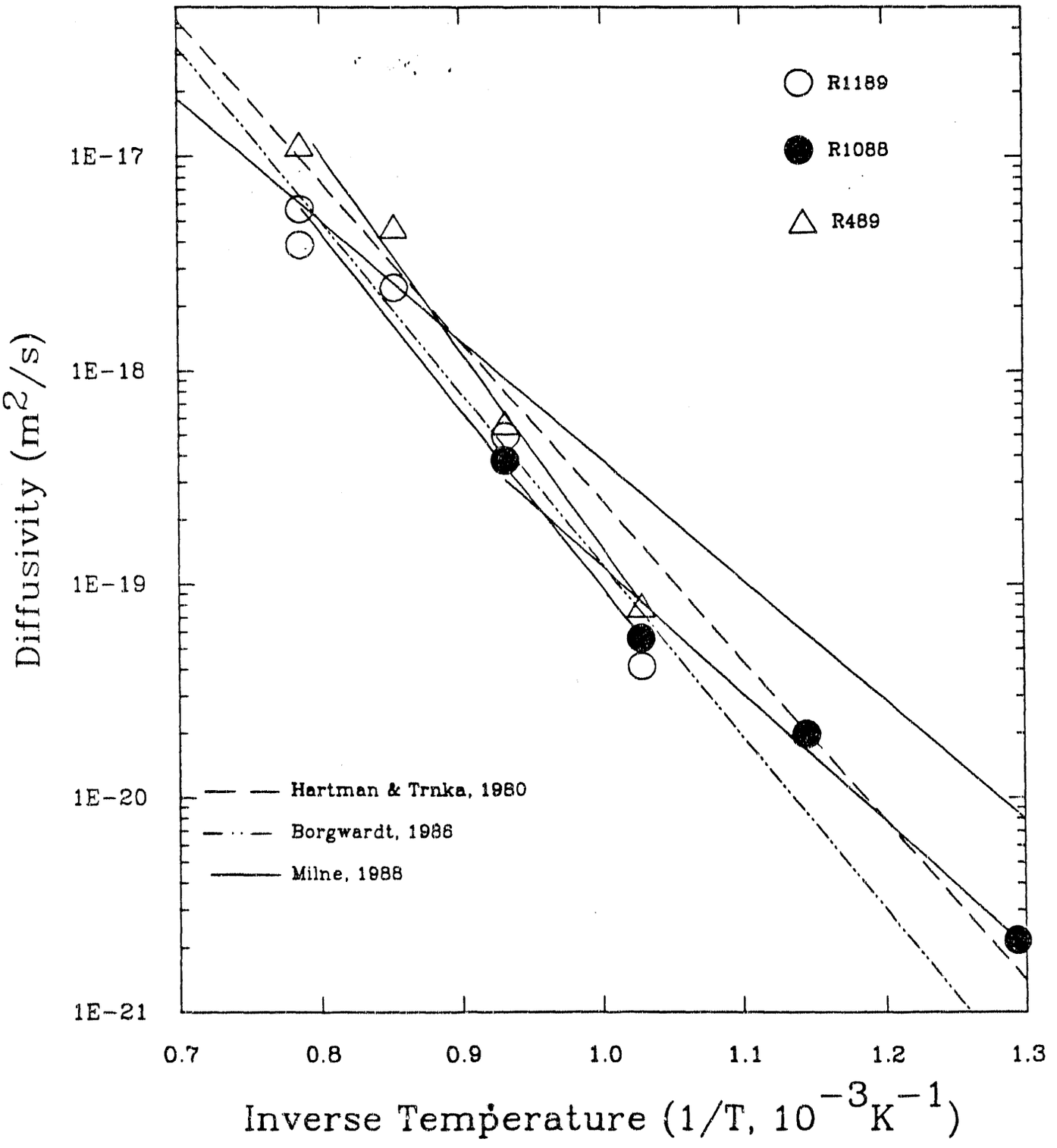

Figure 17. Arrhenius Plot for Lattice Diffusion (D_s^*): Comparison with Literature Results

(a)

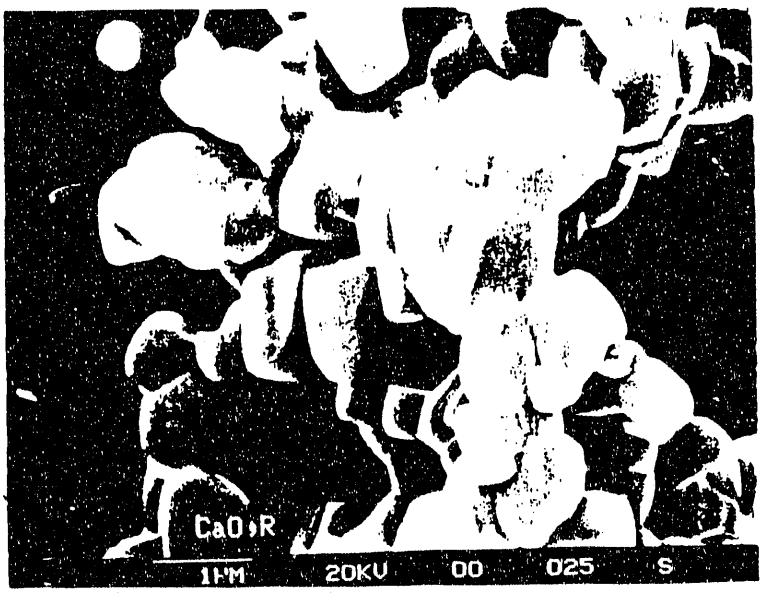

(b)

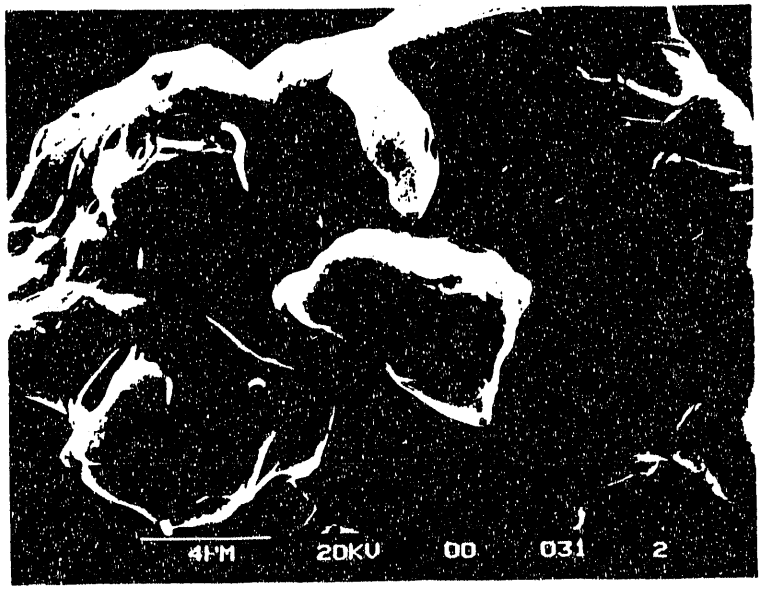

(c)

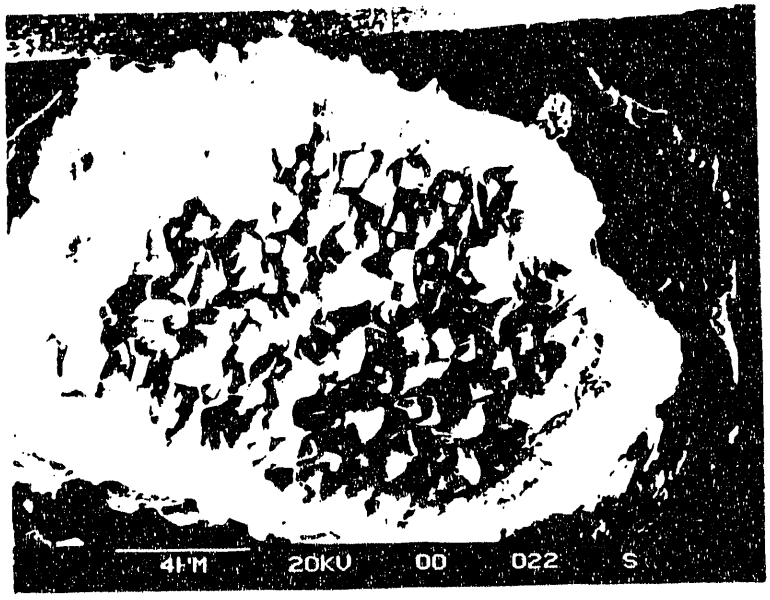

Figure 18. SEM Pictures of Sulfated Limes (after 40 minutes at 800°C):
(a): Synthetic Lime; (b): Single Crystal; (c): Iceland Spar

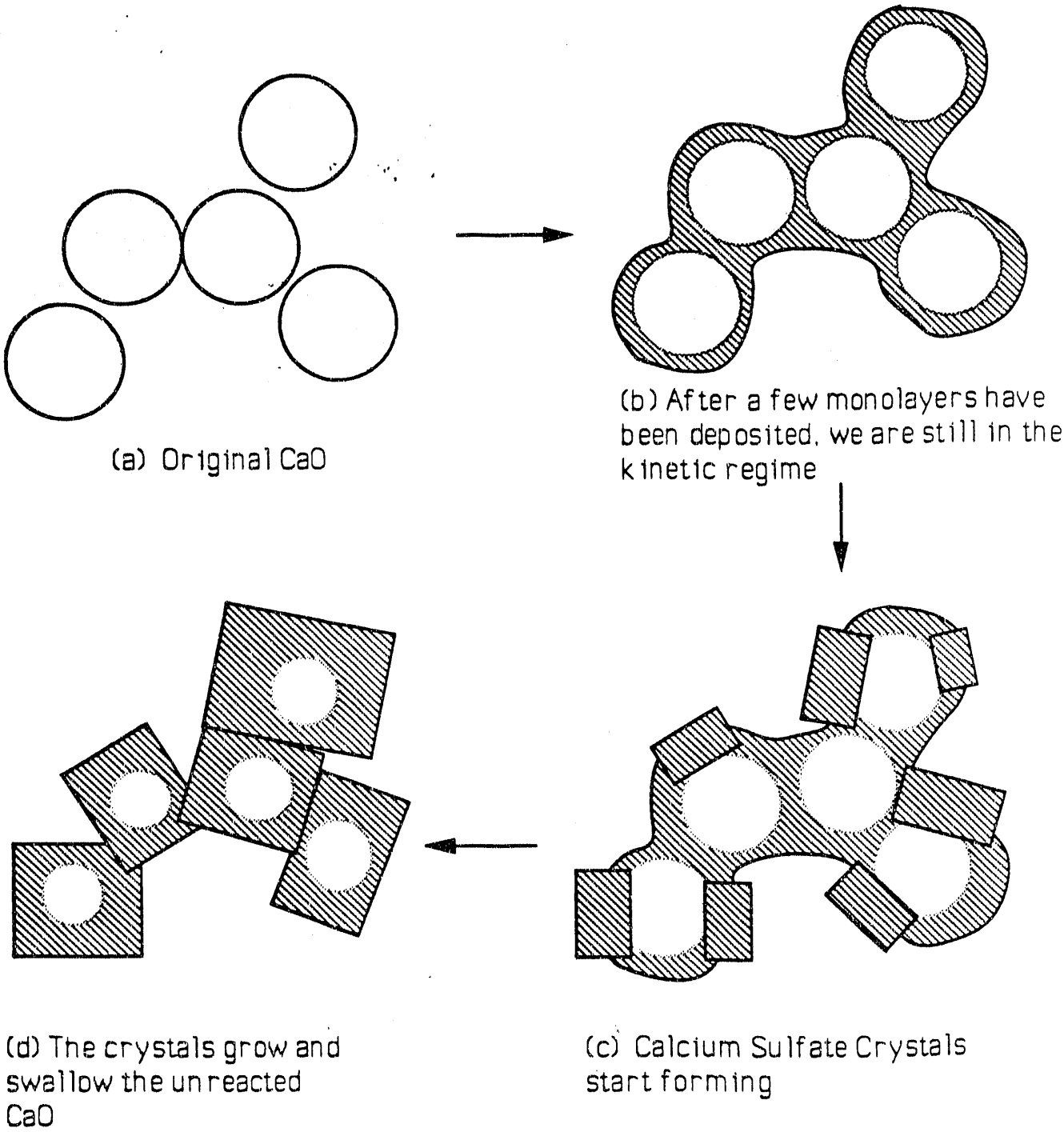

Figure 19. Illustration of the Sulfation of Synthetic Lime

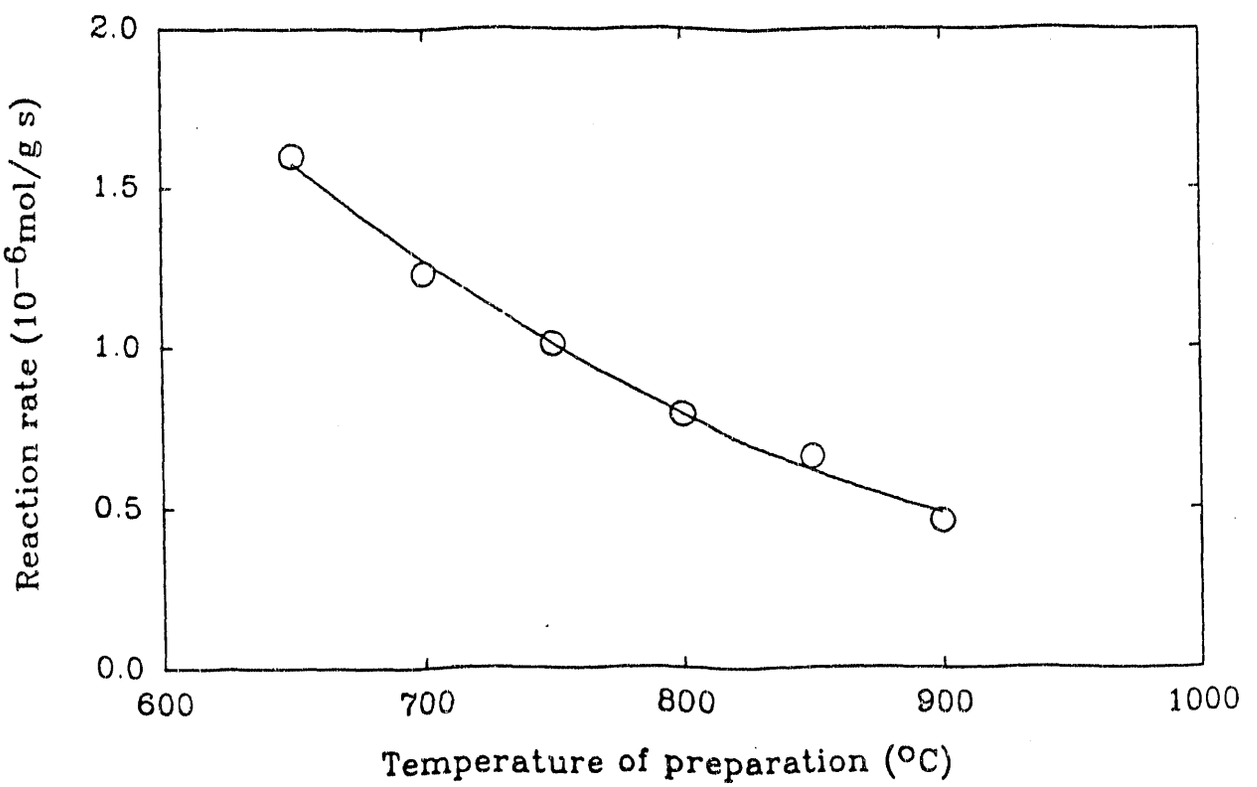

Figure 20. Reaction Rate of Iceland Spar at 800°C after Preparation at Different Temperatures, for Various Amounts of Time such that the Product Layer Thickness is the Same in all Cases (3 minute at 900°C, 5 minutes at 800°C, and 11 minutes at 700°C)

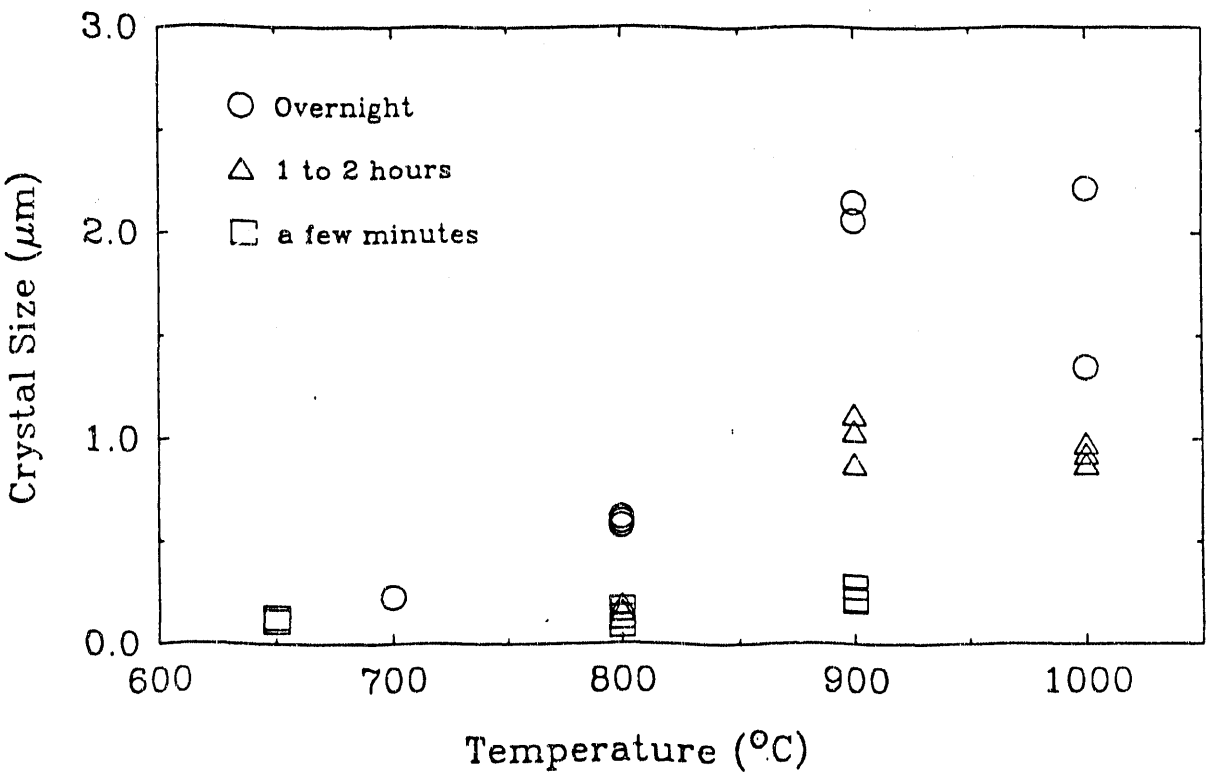

Figure 21. Calcium Sulfate Crystal Size Dependence on Temperature and Time, for Iceland Spar. The Larger Sizes at High Temperature Explain the Results of Figure 20.

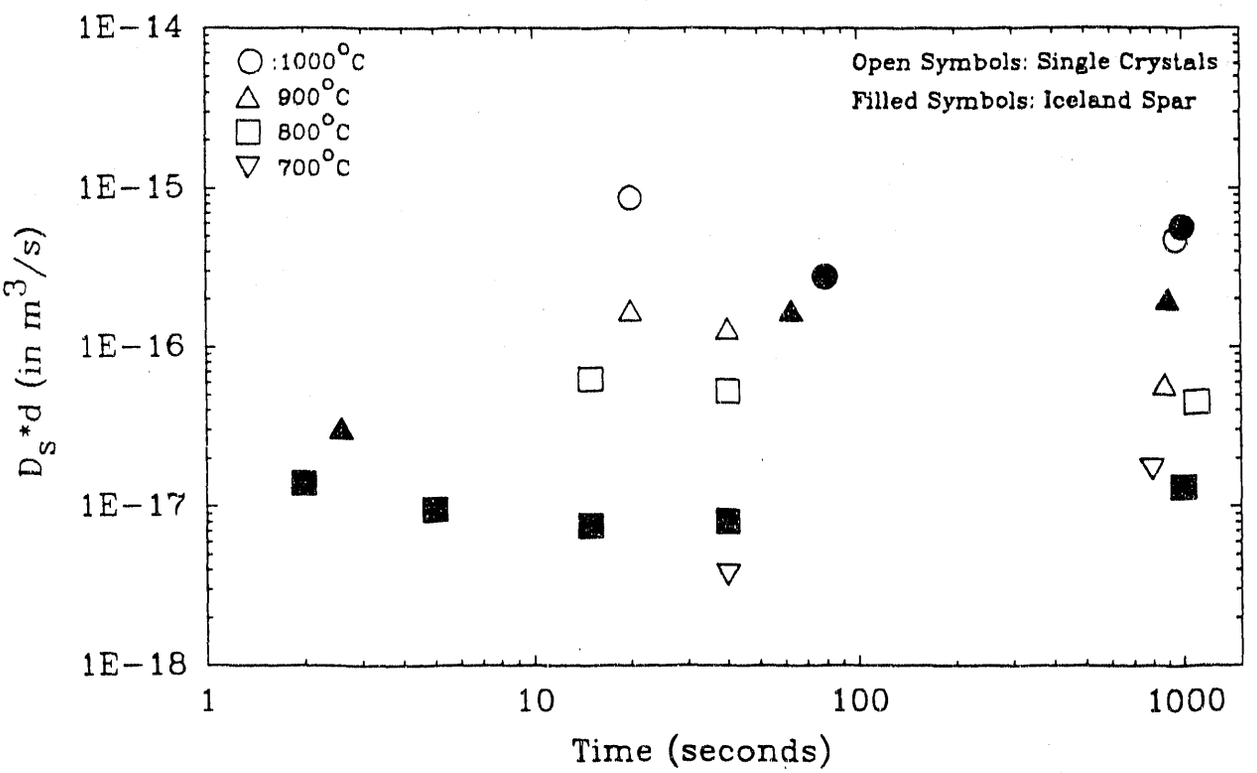

Figure 22. Product of Diffusivity and Product Layer Thickness as a Function of Time and Temperature

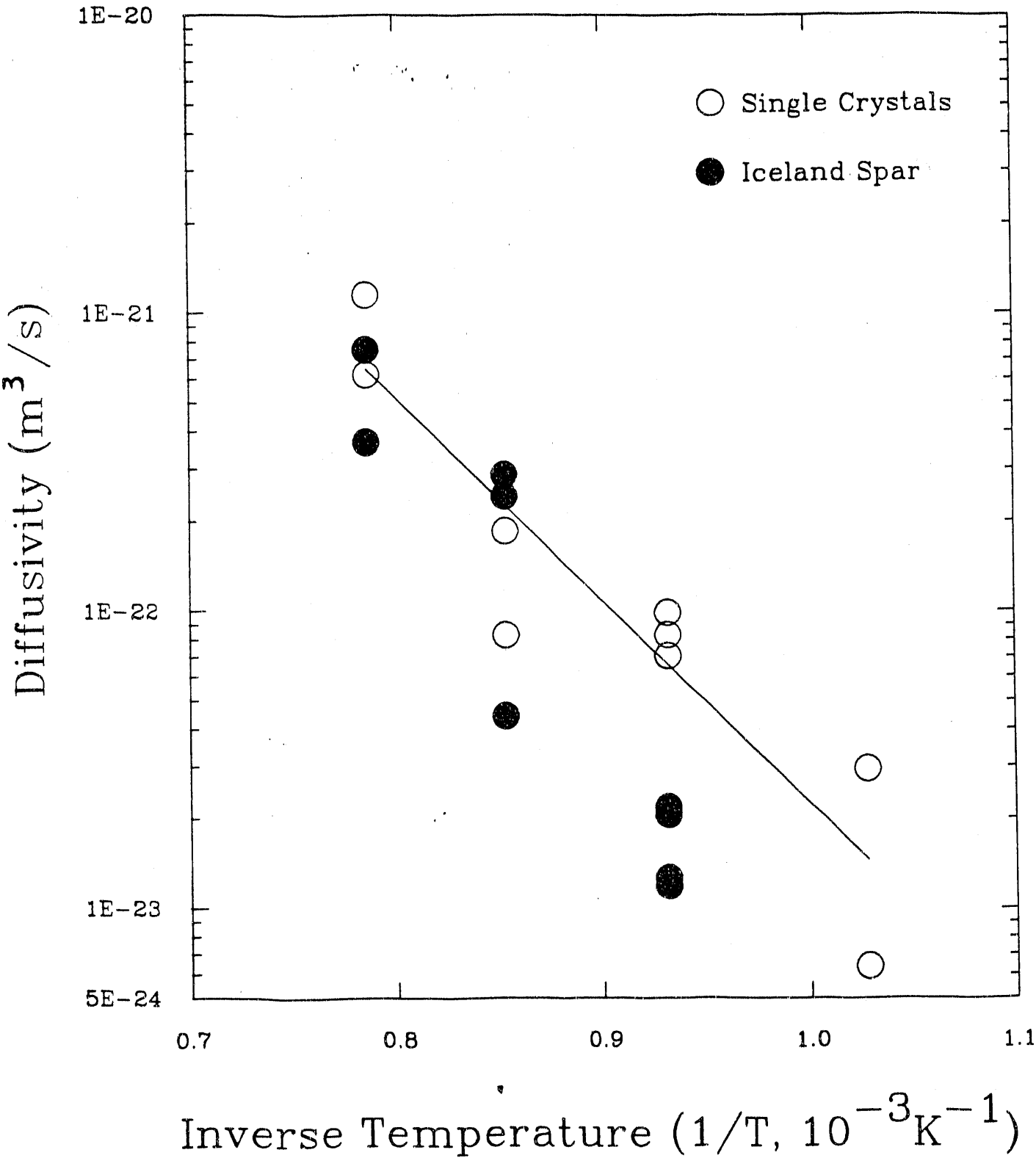

Figure 23. Arrhenius Plot for Crystal Boundary Diffusion, using two different Samples, under 3000ppm SO_2 and 5% O_2

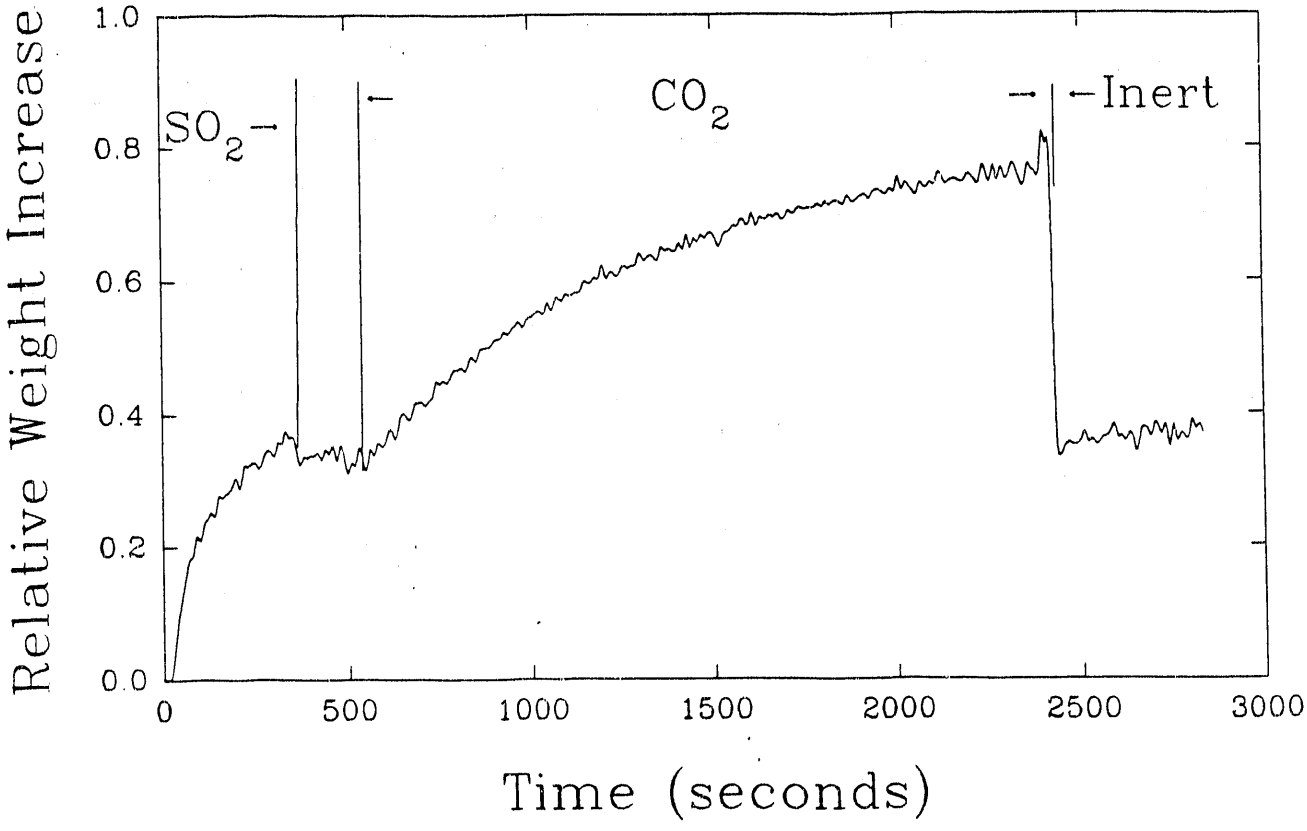

Figure 24. TGA Results of Combination Experiments at 800°C with Synthetic Lime: After Sulfation under 3000ppm SO_2 and 5% O_2 in He, 1 atm CO_2 is introduced.

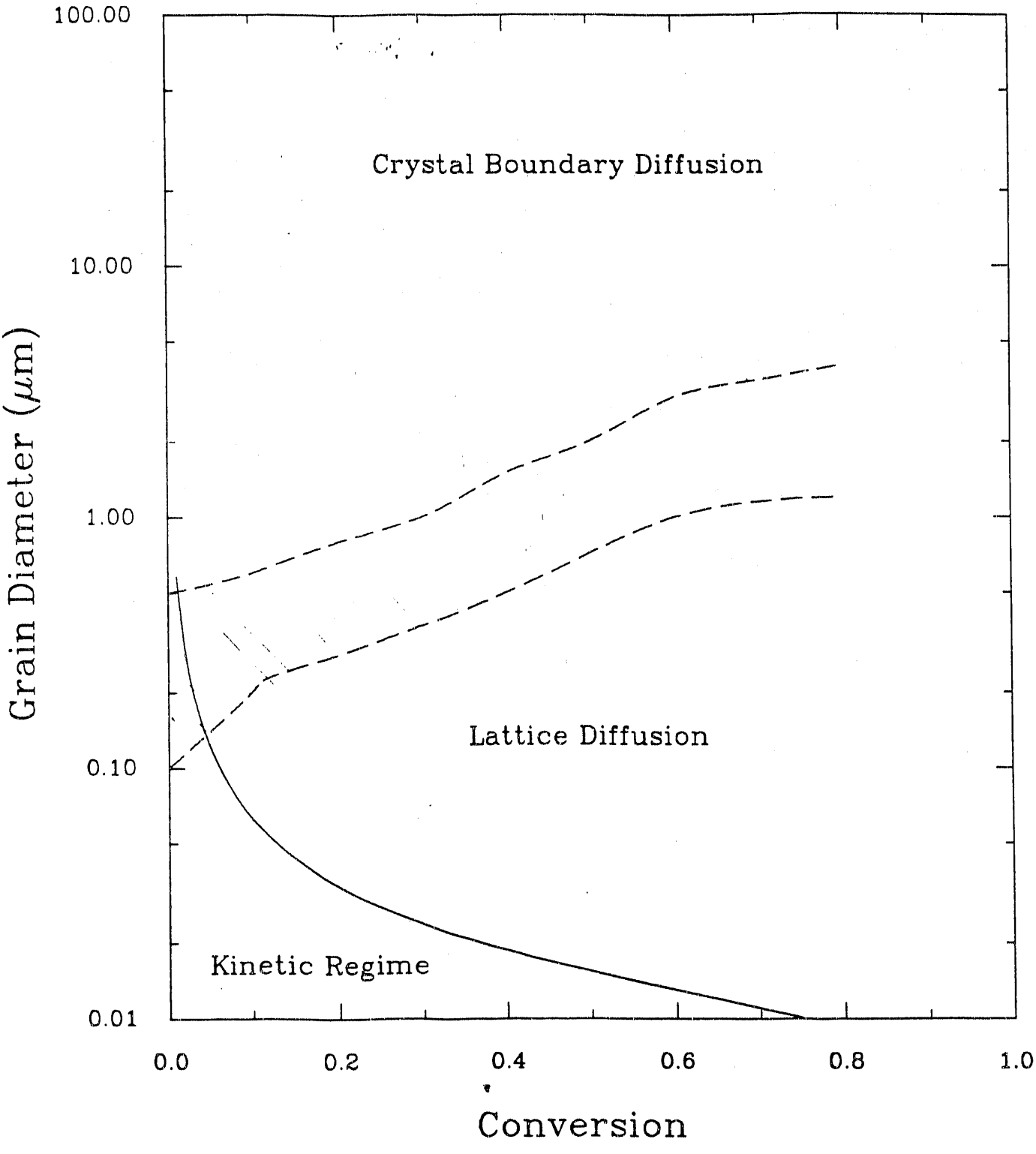

Figure 25. Regime Map Under the Standard Conditions: 3000ppm SO_2, 5% O_2 at 800°C

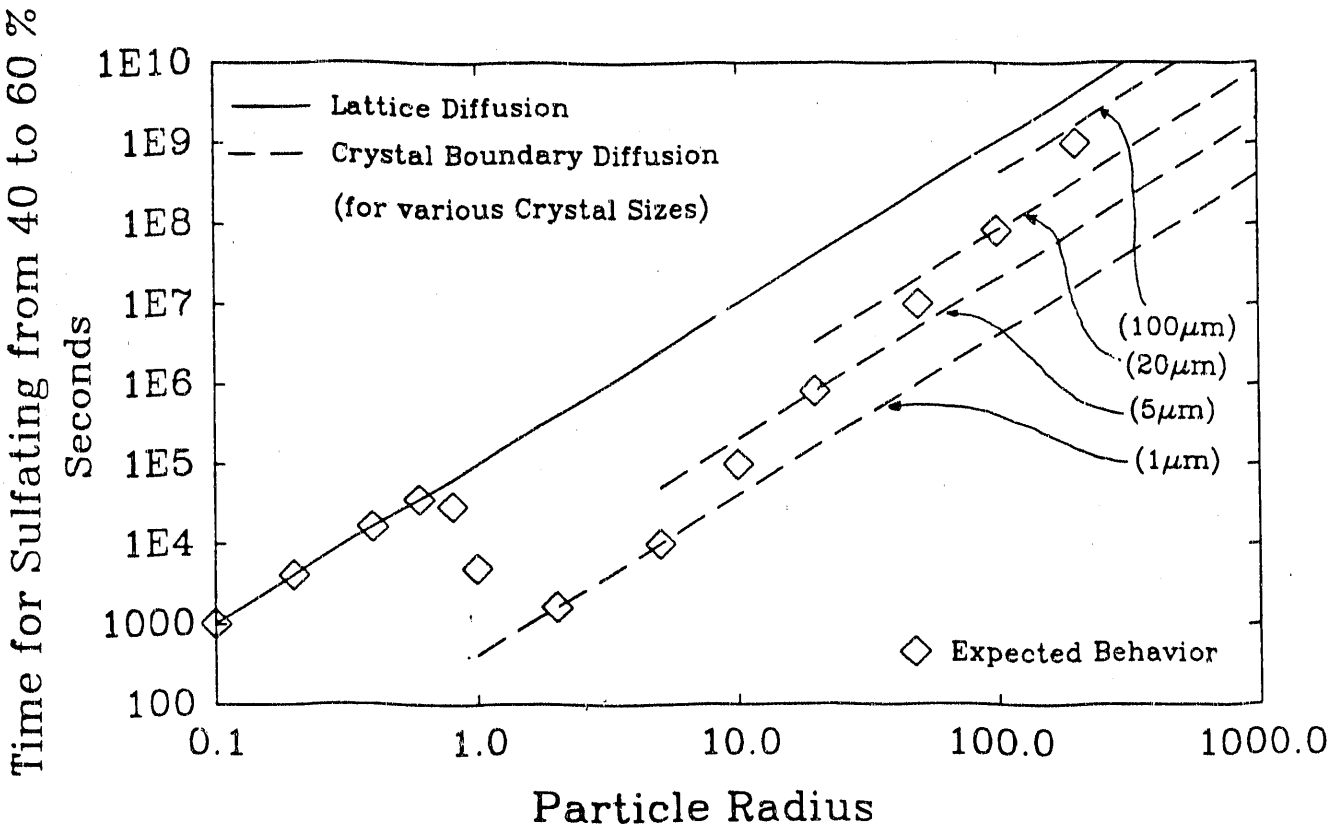

Figure 26. Time needed to increase the conversion from 40 to 60%, in the case of pure lattice diffusion (solid line) or pure crystal boundary diffusion (dashed line). In this last case, the time also depends on the crystal size in the product layer (between brackets). These, sulfate, crystals are expected to be small for small particles and to get the time to grow larger for larger particles. The expected behavior (diamonds) therefore corresponds to crystal boundary diffusion with small grains when the particles are small, and shifts to the diffusion behavior with larger crystals when the particles are larger. When the particles are smaller than 1 μm, lattice diffusion is expected.

END

DATE
FILMED
9/16/92